Structure and substructure in the stellar halo of the Milky Way

Pila Diez, B.

Chapter 5

A search for stellar tidal debris of defunct dwarf galaxies around globular clusters in the inner Galactic halo

Authors

Julio A. Carballo-Bello, Antonio Sollima, David Martínez-Delgado, Berenice Pila-Díez, Ryan Leaman, Jürgen Fliri, Ricardo R. Muñoz, Jesús M. Corral-Santana

Abstract

In the hierarchical formation scenario in which the outer halo of the Milky Way is the result of the continuous accretion of low-mass galaxies, a fraction of the Galactic globular cluster system might have originated in and been accreted with already extinct dwarf galaxies. In this context, we expect that the remnants of these progenitor galaxies might be still populating the surroundings of those accreted globulars. In this work, we present wide-field photometry of a sample of 23 globular clusters in the Galactocentric distance range $10 \leq R_{\rm G} \leq 40\,$kpc, which we use to search for remnants of their hypothetical progenitor systems. Our deep photometry reveals the presence of underlying stellar populations along the line-of-sight of about half of the globulars included in our sample. Among the detections lying in the footprint of the Sagittarius tidal stream, which we identify via the comparison with its orbit derived from numerical simulations, only Whiting 1 and NGC 7492 seem to be inmersed in that remnant at a compatible heliocentric distance. We also confirm the existence of a subjacent Main-Sequence feature in the surroundings of NGC 1851. A tentative detection of the vast Hercules-Aquila cloud is unveiled in the background of NGC 7006.

Published in MNRAS Volume 445, 2971 (2014)

Preprint in arXiv:1409.7390 [astro-ph.GA]

5.1 Introduction

The formation of the outer regions of disc galaxies in the context of the currently most accepted cosmological model, namely Lambda Cold Dark Matter (ΛCDM, Peebles 1974), took place via the hierarchical accretion of minor stellar systems, similar to the nowadays Galactic satellite dwarf galaxies (Font et al. 2011b). Numerical simulations based on this model and focused in our Galaxy (Bullock & Johnston 2005; Cooper et al. 2010; Font et al. 2011a; Gómez et al. 2013) predict that the Galactic halo might be populated by stellar remnants, vestiges of these accretion events. An important observational effort has been made to validate this theoretical work by detecting stellar tidal streams in the halo of the Milky Way.

The first satellite dwarf galaxy discovered that is currently in the process of being accreted is the Sagittarius dwarf spheroidal (Sgr dSph; e.g. Ibata et al. 1994; Bonifacio et al. 2004; Bellazzini et al. 2006b; Siegel et al. 2007) which is following an almost polar orbit around the Galaxy. The destruction of this minor system has generated the largest and most complex halo substructure observed so far (Majewski et al. 2003; Martínez-Delgado et al. 2004a; Belokurov et al. 2006b; Koposov et al. 2012), which has allowed for an investigation of the mass distribution - potential - of the Milky Way by reconstructing its orbit from diverse spectroscopic and photometric datasets (e.g. Law & Majewski 2010b; Peñarrubia et al. 2010). However, there are still significant aspects of this substructure pending for a satisfactory explanation, like the existence of a bifurcation into two parallel streams on its northern section (Fellhauer et al. 2006; Peñarrubia et al. 2011) .

Far from being the only detected tidal debris, wide-sky surveys as the Sloan Digital Sky Survey and the Two Micron All Sky Survey (SDSS and 2MASS respectively; York et al. 2000; Skrutskie et al. 2006), have revealed the existence of substructures such as the Monoceros ring (Newberg et al. 2002; Yanny et al. 2003; Rocha-Pinto et al. 2003; Conn et al. 2005, 2007; Jurić et al. 2008; Sollima et al. 2011), diverse streams such as the Orphan (Grillmair 2006a; Belokurov et al. 2007b; Sales et al. 2008; Newberg et al. 2010), Aquarius (Williams et al. 2011), Cetus (Newberg et al. 2009) and Virgo (Duffau et al. 2006), and the over-densities of Hercules-Aquila (Belokurov et al. 2007a; Simion et al. 2014) and Virgo (Jurić et al. 2008; Martínez-Delgado et al. 2007; Bonaca et al. 2012b) as the best-studied examples. In addition, minor mergers and faint substructures have been observed in spiral galaxies in the Local Universe (e.g. Ibata et al. 2001a, 2007; Martínez-Delgado et al. 2008; McConnachie et al. 2009; Martínez-Delgado et al. 2010b), showing that our Galaxy is not unusual in this respect.

The globular cluster (GC) population of a given galaxy contains valuable information about the formation process of its host galaxy. Evidence for separate populations of GCs in the Milky Way and other galaxies have been steadily accu-

mulating, and it is interpreted as evidence that supports the hierarchical galaxy formation scenario (Zinn 1993; Leaman et al. 2013; Tonini 2013). In their seminal paper Searle & Zinn (1978) showed that while GCs in the inner Galactic halo (at distances < 8 kpc) show a clear radial abundance gradient, GCs in the outer halo do not follow this trend. In terms of the relation between the horizontal branch (HB) type and metallicity found for GCs (and assuming the age as the *second parameter*), Zinn (1993) classified globulars into *old* halo and *young* halo clusters, where the latter would correspond to the accreted fraction of Galactic GCs. Simulations suggest that whereas the outer halo clusters ($R_{\rm G} \geq 15$ kpc) were probably formed in small fragments subsequently accreted by the Galaxy (with the most massive GCs such as Omega Centauri and M 54 as the possible remnant cores of the disrupted progenitor; van den Bergh & Mackey 2004), an inner component of the Milky Way halo (and possibly a fraction of the halo GCs) may have formed *in situ* (e.g. Zolotov et al. 2009). A recent analysis of the relative ages for 55 clusters calculated from the turn-off magnitude (Marín-Franch et al. 2009; VandenBerg et al. 2013) showed that the GCs age-metallicity relation is bifucarted into two distinct groups. Interestingly, these studies find that most of the outer halo GCs belong to the branch characterized by the steeper age-metallicity relation although GCs belonging to both branches cover comparable age ranges.

Among the Milky Way satellites, Fornax and the core of the Sgr dSph host a population of 5 and 4 (at least) GCs respectively (Ibata et al. 1997; Strader et al. 2003), suggesting that accreted low-mass systems might have contributed with their own globulars to the Galactic GC system. The fraction of accreted Galactic clusters estimated by Forbes & Bridges (2010) represents 1/4 of the entire Galactic GC system, when considering parameters such as age-metallicity relations, retrograde orbits and HB morphologies. A higher fraction of $\sim 50\%$ of accreted GCs was estimated by Leaman et al. (2013), which is also consistent with the estimated fraction of accreted halo stars for the Galaxy (Zolotov et al. 2009; Cooper et al. 2013). In this context, we expect part of the Milky Way GC population to be associated with some of the tidal streams that populate the outer halo, similar to what has been observed in M 31, where the location of the outer GC system coincides with the streams observed around that galaxy (Mackey et al. 2010, 2013). If these GCs were formed in subsequently accreted stellar systems, they might be still surrounded by the tidal streams generated by the disruption of their progenitor satellites.

The possible association of Galactic GCs with the stellar tidal stream of Sgr has been extensively considered in the literature using different methods and datasets (e.g. Dinescu et al. 2000; Bellazzini et al. 2002; Martínez-Delgado et al. 2002; Palma et al. 2002a; Forbes et al. 2004; Martínez-Delgado et al. 2004a; Carraro 2009; Forbes & Bridges 2010). Bellazzini et al. (2003) found that, among the Galactic globulars in the distance range $10 \leq R_{\rm G} \leq 40$ kpc, there are at least 18 GCs compatible both in position and kinematics with the orbit proposed for that dSph galaxy by Ibata et al. (1997). More recently, (Law & Majewski 2010a,

hereafter L10) also investigated the association of 64 Galactic GCs with the Sgr stream as predicted by Law & Majewski (2010b). In that case, 9 GCs were suggested as systems formed in the interior of the Sgr dSph, latter accreted by the Milky Way.

The search for Galactic GCs associated with the other possible major accretion event, the Monoceros ring, has been complicated by the uncertainty about the origin and dynamical history of that stellar structure and the unknown location of its tentative progenitor galaxy. Different formation scenarios have been proposed for the stellar ring, from the accretion by the Milky Way of a dwarf companion system (Helmi et al. 2003; Martin et al. 2004; Martínez-Delgado et al. 2005; Peñarrubia et al. 2005; Sollima et al. 2011) to the distortion or detection of more distant Galactic components (Momany et al. 2004; López-Corredoira 2006; Momany et al. 2006; Hammersley & López-Corredoira 2011). Regarding the hypothetical progenitor accreted dwarf galaxy, the controversial Canis Major stellar over-density in the direction $(\ell, b) = (240°, -8°)$ at ~ 7 kpc from the Sun has been proposed as its remnant nucleus (Martin et al. 2004; Dinescu et al. 2005; Martínez-Delgado et al. 2005; Bellazzini et al. 2006b) but its origin has also been the subject of debate during the last years (Momany et al. 2004; Moitinho et al. 2006; Mateu et al. 2009). Nonetheless, several low-latitude GCs have been proposed as members of the Monoceros progenitor galaxy GC system including NGC 1851, NGC 1904, NGC 4590 and Rup 106 (Martin et al. 2004; Forbes & Bridges 2010), NGC 2298 (Crane et al. 2003; Frinchaboy et al. 2004; Martin et al. 2004; Forbes & Bridges 2010) and NGC 7078 (Martin et al. 2004).

In this work, we explore the possibility of the presence of stellar remnants of accreted dwarf galaxies around a sample of GCs in the inner Galactic halo, which have been extensively considered as tracers of the hierarchical formation of the Milky Way halo. With that purpose, we present wide-field deep photometry of a statistically significant sample of clusters and of the area surrounding them.

5.2 Observations and data reduction

5.2.1 Sample selection and observations

The results presented here are part of a systematic survey of stellar tidal debris around GCs of the Galactic halo, based on photometric observations of these systems with wide-field cameras at different intermediate-size telescopes during the last 10 years. Preliminary results of this survey were presented in Martínez-Delgado et al. (2002), Martínez-Delgado et al. (2004a) and Carballo-Bello et al. (2012). In this work, we have focused on clusters lying in the distance range $10 \leq R_{\rm G} \leq 40$ kpc (only 9 Galactic GCs are found beyond that distance), which might include the suggested transition region between accreted and *in-situ* formed Galactic stellar halo ($R_{\rm G} \sim$ 15–20 kpc Carollo et al. 2007). To minimize the presence of disc stars which could severely affect our photometry, we excluded from the initial sample all those clusters at low Galactic latitude ($|b| \leq 20°$) with the exception of NGC 2298 and Rup 106, globulars whose properties suggest an

Table 5.1: Sample of Galactic GCs: positional data, tidal radii and metallicities (Harris 2010; Carballo-Bello et al. 2012).

Cluster	$\ell(^\circ)$	$b(^\circ)$	$d_\odot$(kpc)	R_G(kpc)	r_t (arcmin)	[Fe/H]
Whiting 1	161.2	-60.7	30.1	34.5	3.2	-0.70
NGC 1261	270.5	-52.1	16.3	18.1	10.9	-1.27
NGC 1851	244.5	-35.0	12.1	16.6	11.6	-1.18
NGC 1904	227.2	-29.3	12.9	18.8	11.3	-1.60
NGC 2298	245.6	-16.0	10.8	15.8	10.1	-1.92
NGC 4147	252.8	77.2	19.3	21.4	6.6	-1.80
Rup 106	300.8	11.6	21.2	18.5	9.0	-1.68
NGC 4590	299.6	36.0	10.3	10.2	21.4	-2.23
NGC 5024	332.9	79.7	17.9	18.4	18.0	-2.10
NGC 5053	335.7	78.9	17.4	17.8	13.1	-2.27
NGC 5272	42.2	78.7	10.2	12.0	25.4	-1.50
AM 4	320.3	33.5	32.2	27.8	3.3	-1.30
NGC 5466	42.2	73.6	16.0	16.3	23.4	-1.98
NGC 5634	342.2	49.3	25.2	21.2	9.6	-1.88
NGC 5694	331.1	30.4	35.0	29.4	4.7	-1.98
NGC 5824	332.6	22.1	32.1	25.9	5.7	-1.91
Pal 5	0.8	45.9	23.2	18.6	21.1	-1.41
NGC 6229	73.6	40.3	30.5	29.8	3.8	-1.47
Pal 15	18.8	24.3	45.1	38.4	5.6	-2.07
NGC 6864	20.3	-25.7	20.9	14.7	6.8	-1.29
NGC 7006	63.8	-19.4	41.2	38.5	5.7	-1.52
NGC 7078	65.0	-27.3	10.4	10.4	17.5	-2.37
NGC 7492	53.4	-63.5	26.3	25.3	9.2	-1.78

external origin (Crane et al. 2003; Forbes & Bridges 2010; Dotter et al. 2011). We have also excluded NGC 6715, Terzan 7, Arp 2 and Terzan 8 because their location has already been established within the main body of the Sgr dSph (Bellazzini et al. 2003, 2008) and Pal 12, which has previously been associated to its stream (Dinescu et al. 2000; Martínez-Delgado et al. 2002). Following these criteria, our final sample is composed of 23 of these systems. It represents a half of the GCs in the considered Galactocentric distance range and the 3/4 of the clusters that match our latitude criteria.

Table 5.1 includes the position, distance and other relevant information of our GC sample. The positions and [Fe/H] estimates are taken from the Harris (2010) catalogue. Tidal radii are taken from Carballo-Bello et al. (2012), where structural parameters for these globulars were derived using the same photometric database presented in this paper, with the exception of the clusters Whiting 1, AM 4, Pal 15 and NGC 7006 not included in that work and for which they have been estimated using a similar procedure as the described in Carballo-Bello et al. (2012). The radial density profiles for these 4 GCs have been obtained including information for the inner region of the clusters from the literature (Harris 1991; Trager et al. 1995; Carraro et al. 2007; Carraro 2009).

Our survey strategy was based on obtaining deep photometric observations in a wide field of view (FOV) around the clusters, which allows us to explore for the first time their external regions, poorly represented in shallower photometric data. In this case, the main tracers of the tidal debris of these possible progenitor systems are main-sequence (MS) stars 2–3 magnitudes fainter than the MS turn-off (TO) of the old stellar population. Given the low levels of surface-brightness for known tidal streams ($\mu_V > 30\,\mathrm{mag\,arcsec^{-2}}$, Martínez-Delgado et al. 2001; Majewski et al. 2003), very deep colour-magnitude diagrams (CMDs) are needed to get enough statistic of MS-TO stars in the explored area. In addition, good seeing conditions are essential to undertake a reliable decontamination of background galaxies in the CMD, which would otherwise affect the detection of a MS feature associated to an underlying stellar population in the blue region of the diagram at fainter magnitudes (e.g. see Figures 5.2 and 5.7).

Observations have been performed using the Wide Field Camera (WFC) mounted at the Isaac Newton telescope (INT), established at El Roque de los Muchachos Observatory on the island of La Palma (Canary Islands) and the Wide Field Imager (WFI) at the MPG/ESO2.2 m telescope, at the La Silla Observatory (Chile). The WFC provides, with 4 CCDs with a pixel size of $0.333\,\mathrm{arcsec\,pixel^{-1}}$, a total FOV of 34 arcmin × 34 arcmin. The WFI provides a similar FOV of 34 arcmin × 33 arcmin covered by 8 identical CCDs. A summary of the observations is shown in Table 5.2, including the coordinates of each of the pointings. The typical exposure times were 4×900 s in the B band and 6×600 s in R. The typical seeing was $FWHM < 1''$. Daily sky-flats and bias were obtained and used for bias and flat-field correction by means of reduction routines based on IRAF standard tasks. A set of Landolt (1992) standard stars were observed during the runs, at different airmass ranges to allow a precise calibration of the final photometric catalogs.

Table 5.2: Coordinates, exposure times, mean seeing and dates of the observational campaigns in which the GCs were observed. Service mode observations are denoted by (*s*).

Cluster	RA(2000)	DEC(2000)	t_{exp} B(s)	t_{exp} R/r(s)	seeing(")	Instrument	Obs. run date
Whiting	02:02:56	-03:15:10	4×900	6×600	1.2	WFC	2010/08/17-19
NGC 1261	03:13:41	-55:25:28	4×900	4×600	0.8	WFI	2009/11/08-12
NGC 1851	05:13:04	-39:49:58	3×900	6×600	0.6	WFI	2005/07 (*s*)
	05:15:02	-40:11:57	4×900	6×600	0.8	WFI	2010/02/14-19
NGC 1904	05:23:29	-24:19:21	3×900	5×600	0.5	WFI	2005/07 (*s*)
	05:25:29	-24:19:19	3×900	5×600	0.5	WFI	2005/07 (*s*)
NGC 2298	06:50:05	-35:50:47	4×900	4×600	0.9	WFI	2009/02/19-22
NGC 4147	12:09:40	+18:20:03	4×600	4×600	0.8	WFC	2002/05/15-17
Rup 106	12:38:48	-51:12:36	4×900	6×600	0.9	WFI	2009/02/19-22
NGC 4590	12:38:36	-26:31:45	4×900	6×600	0.8	WFI	2010/02/14-19
NGC 5024	13:12:30	+17:49:59	3×900	3×600	0.7	WFC	2002/05/15-17
NGC 5053	13:16:01	+17:21:51	4×900	6×600	0.6	WFC	2010/06/11-13
NGC 5272	13:41:20	+28:45:32	2×900	3×600	1.1	WFC	2010/05/18 (*s*)
	13:42:11	+28:57:32	3×900	6×600	0.7	WFC	2010/06/11-13
AM 4	13:56:06	-27:19:18	6×900	6×600	0.9	WFI	2009/02/19-22
NGC 5466	14:03:51	+28:16:58	4×900	4×600	0.9	WFC	2008/05/11-12
NGC 5634	14:28:45	-05:45:21	4×900	6×600	0.9	WFI	2010/02/14-19
NGC 5694	14:38:40	-26:21:25	4×900	5×600	0.8	WFI	2010/02/14-19
NGC 5824	15:04:14	-32:53:15	4×900	6×600	1.0	WFI	2010/05/15-19
Pal 5	15:15:41	-00:06:48	2×1000	3×900	0.9	WFC	2001/06/20-27
NGC 6229	16:46:25	+47:20:06	3×900	5×600	1.2	WFC	2010/08/17-19
Pal 15	16:59:36	-00:24:45	4×900	6×600	0.9	WFI	2010/05/15-19
NGC 6864	20:05:46	-21:41:30	3×900	6×600	0.5	WFI	2010/05/15-19
NGC 7006	21:01:29	+16:11:15	4×900	4×600	1.0	WFC	2001/06/22-28
	21:08:48	+18:24:51	3×900	4×600	0.9	WFC	2001/06/22-28
NGC 7078	21:29:36	+12:09:00	3×900	6×600	1.0	WFC	2010/06/11-13
	21:29:58	+12:40:00	4×900	6×600	0.8	WFC	2010/06/11-13
NGC 7492	23:09:16	-15:49:14	4×900	5×600	0.9	WFI	2009/11/08-12

5.2.2 Photometry and completeness test

PSF photometry was obtained using DAOPHOT II/ALLSTAR (Stetson 1987) Our final catalogs only contains objects with |SHARP| ≤ 0.4, reducing the pollution in the CMDs by background galaxies and allowing us to detect the MS of the tentative underlying streams in the region of the diagram dominated by these non-stellar objects. The aperture correction of our magnitudes were performed using bright stellar-shaped objects in the outer regions of the field, far from the GC, with $\sigma < 0.1$. With these criteria, we had a good sample of bright stars to compare the PSF fitting from ALLSTAR with the aperture photometry obtained with DAOPHOT II/PHOT. The typical corrections are below 0.2 mag. To estimate the magnitude of our stars outside the atmosphere, we used the extinction coefficients computed for each observatory: $A_{\rm B} = 0.22$ and $A_{\rm r} = 0.07$ magnitudes per airmass unit for the Roque de los Muchachos Observatory and $A_{\rm B} = 0.19$ and $A_{\rm R} = 0.06$ at La Silla Observatory.

For the calibration of the WFC photometry, we have searched for stars present both in our data and in SDSS. Due to the differences between the filters used by this survey and those used in our project, we transformed the SDSS magnitudes (*ugriz*) to the Johnson-Cousins system (*BR*) using Chonis & Gaskell (2008) equations (for stars in the color range $0.08 < r - i < 0.5$ and $0.2 < g - r < 1.4$). The brightest subsample of common stars (20–30 stars per chip) was used to obtain a correction factor to apply to our objects and that also accounts for the differences between the photometric systems. No significant color trends have been noticed in the comparison between B and R magnitudes in the WFC and Johnson-Cousin photometric system. For this reason we applied only a systematic shift. Mean values for these corrections are found to be $C_{\rm B} = 25.10 \pm 0.08$ and $C_{\rm R} = 25.72 \pm 0.09$. For the WFI data, we derived transformations from the comparison of the instrumental results for the Landolt (1992) standard stars observed and their calibrated magnitudes. The mean values for the transformation coefficients are:

$$B_{Lan} - B_{inst} = 25.09\,(\pm 0.09\,) + 0.19\,(\pm 0.23\,)\,(B-R)_{inst} \tag{5.1}$$

$$R_{Lan} - R_{inst} = 24.57\,(\pm 0.07\,) - 0.02\,(\pm 0.02\,)\,(B-R)_{inst} \tag{5.2}$$

In order to estimate the completeness of our photometric catalogs in the surrounding area of the clusters, we have considered separately the furthest chip with respect to the cluster centre. We have included in the images synthetic stars with magnitudes in the range $17 \leq B, R \leq 26$ and color $0.5 < B - R < 1.5$, randomly distributed throughout the chip. The total number of synthetic stars added in each of the frames was designed not to exceed 15% of the number of originally

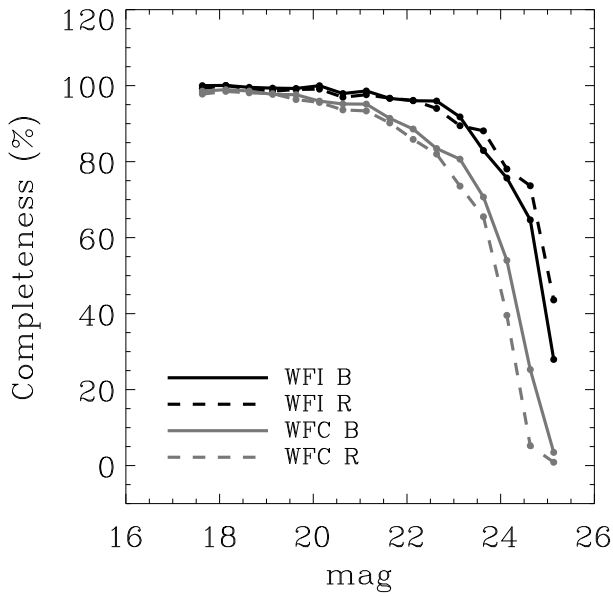

Figure 5.1: Examples of the photometric completeness obtained in this work for the B (solid line) and R (dashed line) bands as a function of the magnitude for WFC (grey) and WFI (black), for the clusters NGC 6229 and NGC 5634 respectively. Synthetic stars with magnitudes below 22 in the WFI are completely recovered, while that percentage drops below 80% at $B, R \sim 24$. As for the WFC photometry, a completeness of 80% is derived up to magnitudes $B, R \sim 23.5$, while it drops to the 60% at $B, R \sim 24$. All the magnitudes are in the Johnson-Cousins system.

observed sources and have been placed in separated cells to avoid self-crowding. For each of the globulars, we obtained 50 of these altered images and they were processed with DAOPHOT II using the same PSF model derived for the observed stars.

We estimated the fraction of synthetic stars recovered by ALLSTAR for all the images and derived a mean variation of that fraction as a function of the magnitude. In Figure 5.1 it is shown the percentage of recovered stars for the B and R bands, corresponding to one of the outer chips in the mosaics obtained for two clusters with typical exposure times and seeing (see Table 5.2), but observed with different instruments. Our results show a similar behaviour for both bands but with small differences between the instruments. On the one hand, our WFI photometry recovers around the 100% of the synthetic stars up to magnitudes $B, R \sim 22$ and in that case the completeness drops marginally below 80% at $B, R \sim 24$. For the WFC, considering the same magnitudes ranges defined above,

we obtained a 90 and 60% of completeness for $B, R \sim 22$ and 24 respectively. Despite these differences regarding the number of recovered sources in both instruments, we conclude that, given the depth of our data, our photometry should be able to detect the presence of subjacent tidal streams if they are present in the surroundings of these GCs. Hereafter we define $< V >= (B + R)/2$.

5.3 Methodology

There are several scenarios where one might expect to observe apparent tidal debris around Galactic halo GCs: *i)* the GC could itself be in the process of tidal disruption due to the tidal field of the Milky Way (e.g. Pal 5; Odenkirchen et al. 2001, 2003), *ii)* the tidal debris could originate from the disruption of the relic of the galaxy that originally hosted the cluster (as is the case with the Sgr dwarf GCs and almost certainly those seen apparently embedded in tidal substructures in and around M 31 (Mackey et al. 2013) and *iii)* the GC could by chance be superimposed in projection against other large-scale halo substructure.

Here, we focus on the detection of debris from a subjacent galaxy remnant. A complete confirmation of such association between GCs and tidal stream would require follow-up spectroscopy (e.g. velocities, chemical tagging) for the members of these tidal debris. With photometry only it is not possible to differentiate between these scenarios, so our results are a first step to identify those Galactic GCs possibly accreted.

5.3.1 Selection of the extra-tidal field of the cluster

An important issue in this work is to estimate the tidal edge of the cluster and separate the possible stellar remnants from the GC stellar content. Tidal radii, commonly denoted by $r_{\rm t}$, are key structural parameters in King models (King 1966) and indicate the distance at which the radial density profile reaches the theoretical zero level. It has been classically used as the physical edge of a GC and all those stars lying beyond this distance have been typically classified as *extra-tidal* content. Carballo-Bello et al. (2012) found that when MS stars are included to derive a more complete radial density profile, the derived $r_{\rm t}$ are a 40% bigger on average than those derived from shallower photometry. Moreover, in many cases the overall shape of the density profile is not well reproduced by King models, especially in the outer parts of the cluster. This indicates that $r_{\rm t}$ is only a rough estimate of the edge of a cluster (see also McLaughlin & van der Marel 2005) and by assuming it as the separation between cluster and fore/background stellar populations, the CMD corresponding to the latter might be still populated by cluster members.

Figure 5.2 illustrates the importance of using that selection criteria in the obtention of the CMDs for the fore/background stellar populations. We have generated both the diagrams corresponding to the stars beyond the tidal radius of NGC 5694 set at $r_{\rm t} = 4.7$ arcmin and $1.5\,r_{\rm t}$, using in this case the value derived from the profiles obtained in Carballo-Bello et al. (2012). It is apparent

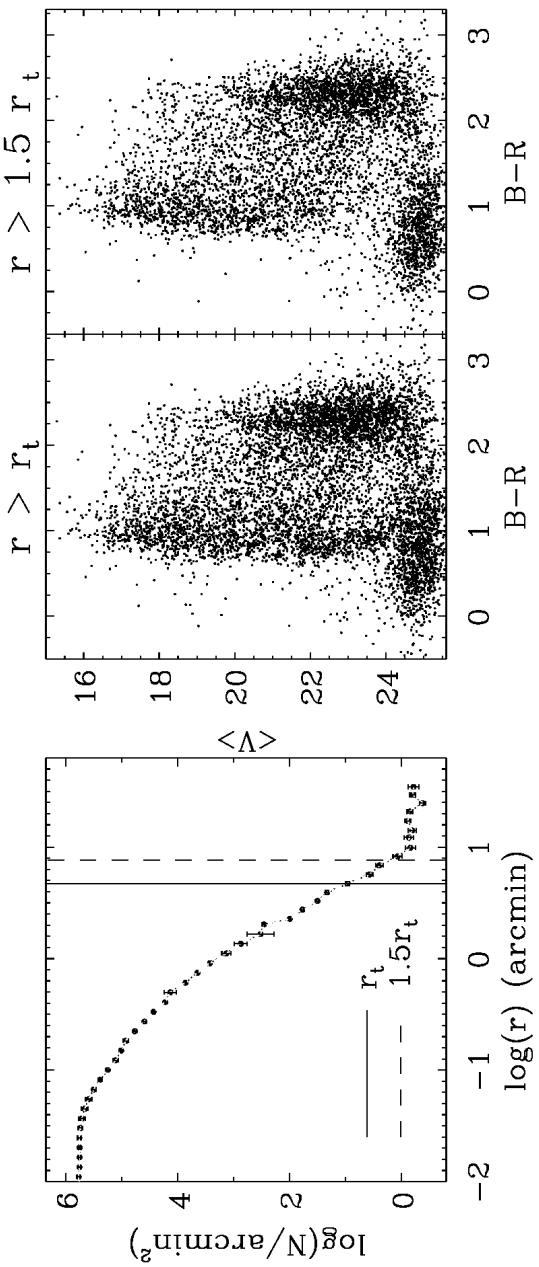

Figure 5.2: Left: radial density profile derived by Carballo-Bello et al. (2012) for NGC 5694, where the vertical lines indicate the position of the King tidal radius (r_t) derived on that work and 1.5 times that distance from the cluster centre. The middle and right panels correspond to the CMDs generated with the stars beyond those distances from the cluster centre. When stars beyond the tidal radius are considered, the CMD shows an over-density associated with the presence of NGC 5694 stars as expected from the position of r_t in relation to the derived radial profile.

that the King tidal radius lies within the outer part of the GC profile, so the contribution of NGC 5694 stars becomes important even outside this distance. On the contrary, when the distance at which the radial density remains nearly constant is considered, the over-density associated to the GC content is not present in the diagram. Trying to avoid as much as possible the contamination by GC stars, our criterion for this separation was set on 1.5 times the formal King tidal radius $r_{\rm t}$, in most cases this coincides with the distance at which the radial density reaches the background level. We adopted the tidal radii determined in Carballo-Bello et al. (2012) using the present photometric dataset (listed in Table 5.1). For the clusters Whiting 1, AM 4, Pal 15 and NGC 7006, not included in the above work, we determined tidal radii using the same procedure described in Carballo-Bello et al. (2012). Hereafter, we define $r_{bg} = 1.5\,r_{\rm t}$. Figures 5.3 to 5.6 show the radial density profiles of our target clusters where the adopted value of r_{bg} is indicated.

Unfortunately, because of the relatively small extra-area and limited angular coverage of our data we are not able to detect any large-scale gradient and/or asymmetry in the distribution of extra-tidal area.

5.3.2 Identification of tidal debris in wide-field photometry with Milky Way synthetic colour-magnitude diagrams

Galactic tidal streams are highly dispersed resulting in a low surface-brightness structure that generates a modest representation of more evolved stars in the CMDs. Thus, we expect that the only feature that may indicate the presence of a stream around a GC is the presence of a MS that might be coincident with that of the GC if they lie at the same distance. However, the same feature could be present if the cluster has developed tidal tails because of its interaction with the Milky Way. In the majority of the cases, the MS stars from the subjacent tidal remnant are hidden in the CMD due to the combination of the contributions of a minor fraction of cluster members, fore/background stellar populations from the different Milky Way components (mainly the disc and halo) and background galaxies.

The best method to correct from these contribution is to obtain observations of adjacent control fields with similar Galactic latitude but several degrees away from the GCs, with similar FOV and exposure time than the target fields. However, we could not obtain these kind of observations during the observing time granted for this project. For this reason, to disentangle the Milky Way stellar halo contribution and to identify any subjacent population, we compared the observed diagrams with synthetic CMDs for the same line-of-sight of each cluster and for a similar solid angle computed assuming a Milky Way model. In this work, we have considered the TRILEGAL (Girardi et al. 2005; Vanhollebeke et al. 2009) and Besançon (Robin et al. 2003) Milky Way models, that provides public available webpage scripts to compute simulated CMDs in selected Galactic fields.

Figure 5.7 shows a CMD observed for one of the GCs in our sample (NGC 2298), together with the diagrams obtained with the two models, for the same direction

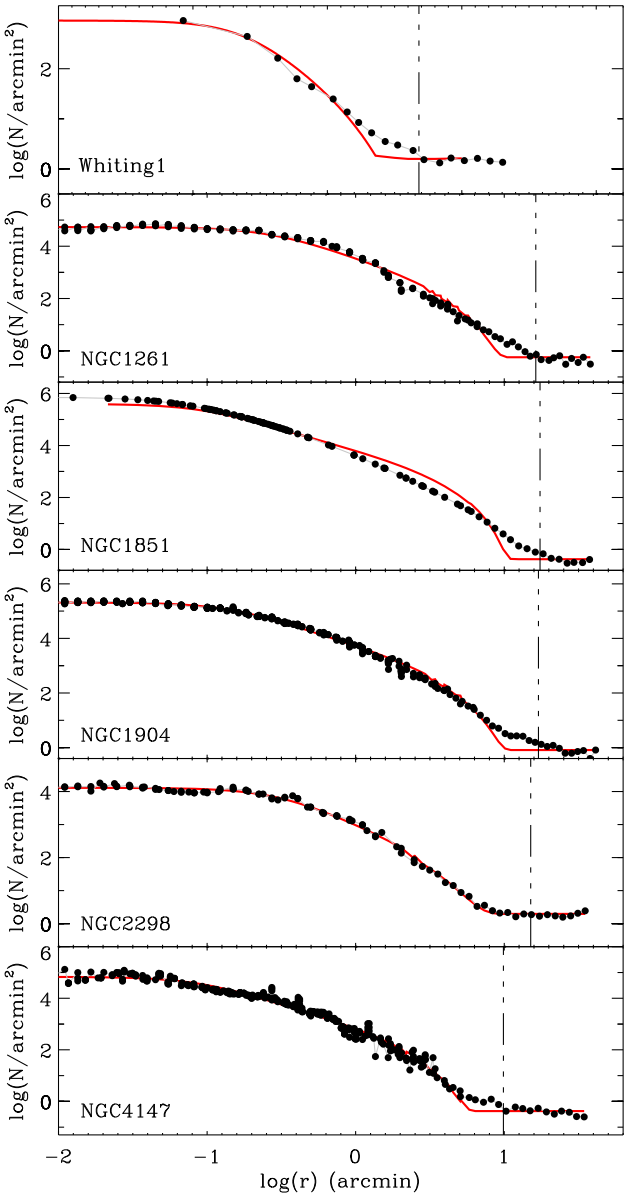

Figure 5.3: Radial density profiles as derived by for Whit 1, NGC 1261, NGC 1851, NGC 1904, NGC 2298 and NGC 4147. The vertical line indicate the distances from the cluster centre where the cluster content has been separated from the rest of objects in the photometric catalogues. The red line corresponds with the best King model fitting (Carballo-Bello et al. 2012).

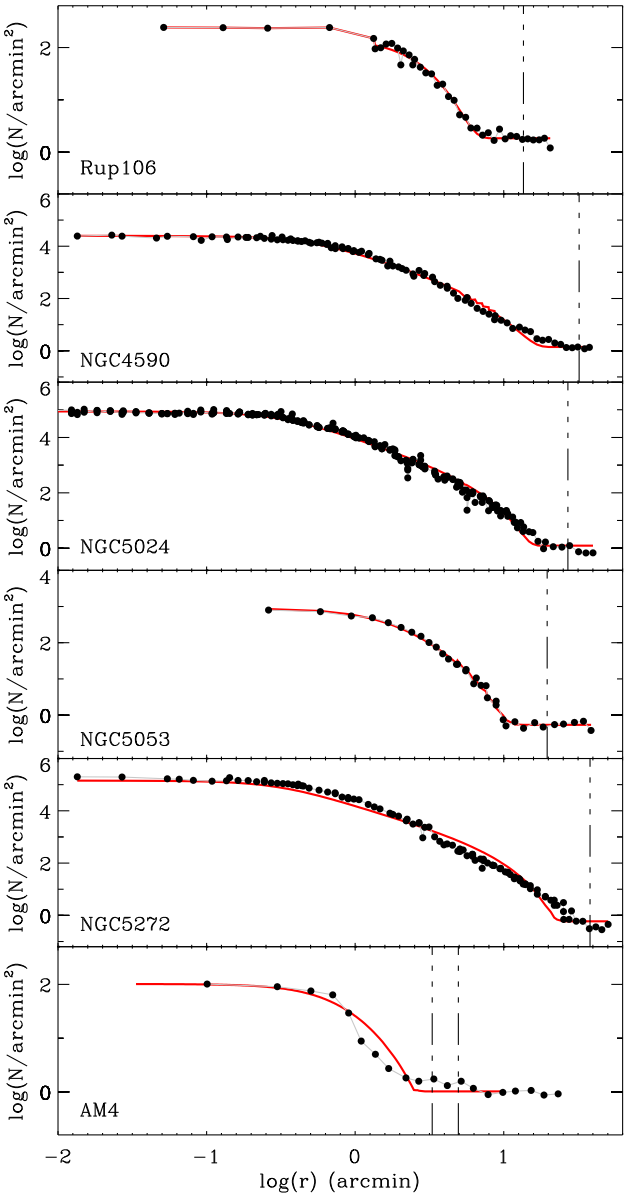

Figure 5.4: Radial density profiles as derived by for Rup 106, NGC 4590, NGC 5024, NGC 5053 and AM 4. The vertical line indicate the distances from the cluster centre where the cluster content has been separated from the rest of objects in the photometric catalogues. The red line corresponds with the best King model fitting (Carballo-Bello et al. 2012).

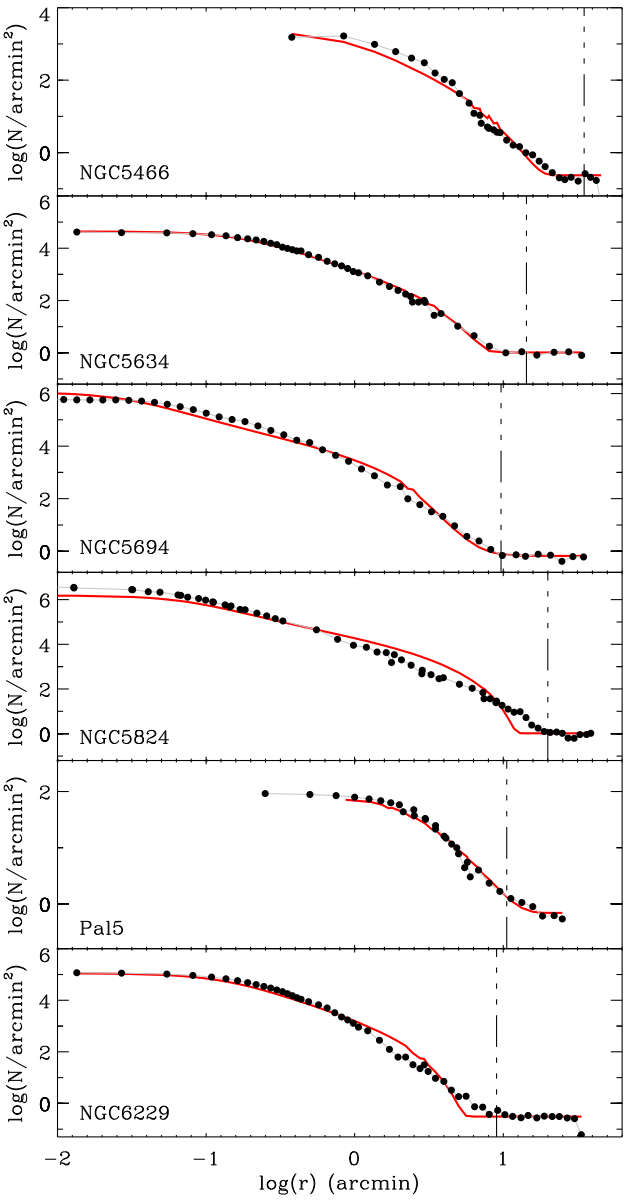

Figure 5.5: Radial density profiles as derived by for NGC 5466, NGC 5634, NGC 5694, NGC 5824, Pal 5 and NGC 6229. The vertical line indicate the distances from the cluster centre where the cluster content has been separated from the rest of objects in the photometric catalogues. The red line corresponds with the best King model fitting (Carballo-Bello et al. 2012).

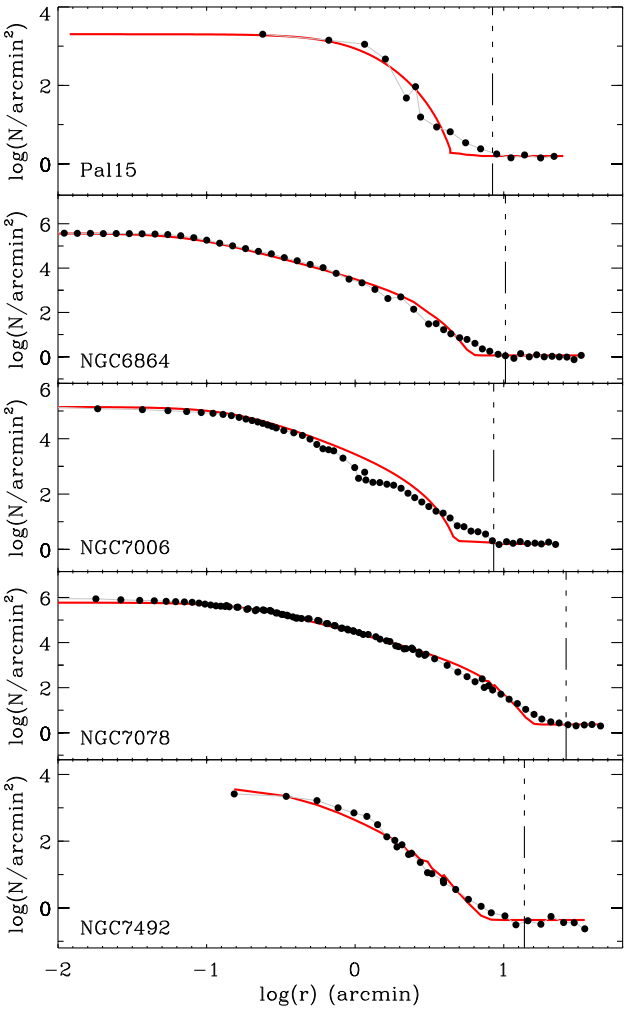

Figure 5.6: Radial density profiles as derived by for Pal 15, NGC 6864, NGC 7006, NGC 7078 and NGC 7492. The vertical line indicate the distances from the cluster centre where the cluster content has been separated from the rest of objects in the photometric catalogues. The red line corresponds with the best King model fitting (Carballo-Bello et al. 2012).

in the sky. This comparison allows us to identify the over-density of objects in the bluer region of the diagram, around $V \sim 24$, as background galaxies, a characteristic feature in wide-field photometry. The differences observed between the synthetic CMDs clearly indicate that the choice of the Milky Way model for comparison would play a relevant role in the detection of Galactic substructures. In that figure, we have delimited a region in the CMD that encompasses the component associated with the Galactic halo, in which this study is focused, defined by $0.6 < B - R < 1.5$ and $21 < V < 23.5$. This clearly shows that the Besançon model predicts a larger number of stellar halo stars than TRILEGAL, affecting the significance of any eventual tidal debris

We have compared the stellar content of TRILEGAL/Besançon in that box of the CMDs for different sections of the Galactic halo. We have obtained 12 synthetic CMDs using both models with an area $\Omega = 0.25\,\mathrm{deg}^2$ for the Galactic longitudes $\ell = 0$, 90 and 180° and latitudes $b = 25$, 40, 60 and 90°. The number of predicted halo stars in that box, for all the directions in the sky considered, is larger for the Besançon results. For $\ell = 180°$ and $\ell = 90°$ we find a similar behaviour, showing that the contribution of halo stars in the TRILEGAL model with respect to Besançon is considerably lower with $\mathrm{N_T/N_B} \sim 0.3-0.4$, where $\mathrm{N_T}$ and $\mathrm{N_B}$ represent the star counts in that box for TRILEGAL and Besançon, respectively. These differences might arise from the different structural parameters assumed by these models to describe the Galactic stellar halo. On the one hand, the TRILEGAL model allows the user to select between a $r^{1/4}$ and an oblate $r^{1/4}$ stellar halo distribution, where in the latter case the oblateness parameter q_h remains as free parameter. Instead, in the Besançon model, the spheroid component is described by a power-law with slope $\alpha = -2.44$ with a fixed value for the oblateness set at $q_\mathrm{h} = 0.76$.

Gao et al. (2013) has recently studied the ability of these models to reproduce Hess diagrams generated from SDSS data in a specific area of the sky. Although in their results both models show problems to reproduce the observations, the section of the CMD dominated by halo stars - area of interest for this work - was more adequately represented by the synthetic diagrams generated by TRILEGAL. Given these significant differences in the contribution of halo stars, we will continue using as reference both the CMDs generated with TRILEGAL and Besançon, although new incoming versions of these models, fitting the parameters to wide-sky surveys (e.g. Robin et al. in preparation), will have to be taken into account in future searches for halo substructures.

To estimate the significance of the detections in our photometry, we have compared the observed stellar counts with those computed from the synthetic CMDs generated with TRILEGAL for the same line-of-sight and solid angle. The input parameters for that model are taken from the optimization obtained by Gao et al. (2013) (see Table 3 on that paper). For the Besançon model, we have used the default parameters. The observed stars considered to derive the significance of a subjacent population are those contained between the V-level of the TO and the level where the CMD is dominated by background galaxies, with a difference

in colour $0.1 < \delta(B-R) < 0.2$ with respect to the corresponding isochrone (see Section 5.3.4). Assuming the uncertainty in the number counts as $\sigma_{\rm N} = \sqrt{N}$, the significance is given by

$$S = \frac{(\mathrm{N_{CMD}} - \mathrm{N_{model}})}{\sqrt{\mathrm{N_{CMD}} + \mathrm{N_{model}}}} \tag{5.3}$$

where $N_{\rm CMD}$ is the number of observed stars following the criteria described above and $N_{\rm model}$ the TRILEGAL/Besançon counts in the same area of the synthetic CMD after correcting for completness. In this work, S will indicate the significance of the detections with respect to the synthetic model. Given the uncertainties linked to the performances of the Galactic models in reproducing the real Galactic field population we defined a conservative treshold for a positive detection of an underlying stellar population when $S > 5$.

Our ability to detect the presence of stellar substructures with surface-brightness comparable to those of Galactic tidal streams is also affected by the position of the fields. It is possible to estimate the surface-brightness detection limit of our method to detect a Sgr-like stellar population that stands out with $S = 5$ above the Galactic stellar populations and as a function of the direction in the sky. We have used the distance-dependent expression proposed by Bellazzini et al. (2006a):

$$\mu_V = -2.5\log(n) + 2.5\log(\Omega) + (m-M)_0 + K \tag{5.4}$$

where n is the number of MS stars, Ω the solid angle observed, $(m-M)_0$ the distance modulus to the stellar population and K includes theoretical elements (see the complete formula in Bellazzini's paper). We have calibrated the latter term applying this expression to the subjacent Sgr population unveiled around Whiting 1, and using a surface-brightness for that portion of the stream of $\mu_{\rm V} = 30.6\,\mathrm{mag\,arcsec^{-2}}$, measured by (Koposov et al. 2012). We define a box in the CMD including all the stars in the subjacent MS to determine K - assuming the same heliocentric distance that of Whiting 1 - and used that box in the synthetic CMDs used in Section 5.3.2 to count the number of stars predicted by TRILEGAL (after correcting for incompletness). After that, we estimated the necessary number of stars in that box to obtain a $S = 5$ detection above the fore/background population using Equation 5.3 and translate those counts into surface-brightness by applying Equation 5.4, assuming the same distance modulus of Whiting 1.

Figure 5.8 shows the limiting surface-brightness (5σ detection) as a function of b and for the ℓ values considered above. As expected, we will be able to detect the presence of fainter halo substructures at higher Galactic latitudes, where the halo component becomes less important in the obtained CMDs. A tidal stream as the one found around Whiting 1 would be detected in the area $b > 80^\circ$ for all ℓ, when the surface-brightness of that structure is as faint as $31.5 < \mu_{\rm V} < 32\,\mathrm{mag\,arcsec^{-2}}$. The surface-brightness required for a tidal stream to

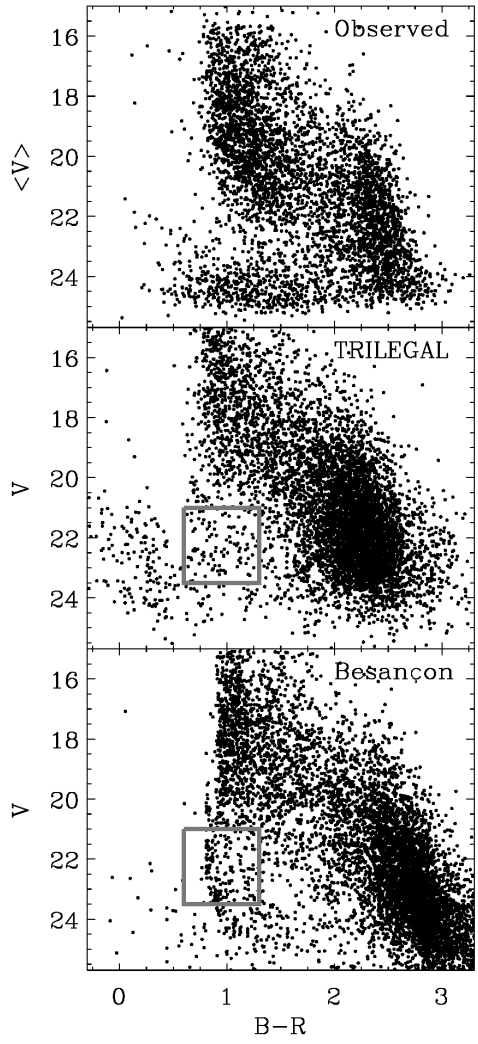

Figure 5.7: Top: example of CMD obtained for the surroundings of NGC 2298 for stars beyond $r_{\rm bg}$ from the cluster centre. Middle and bottom panels: CMDs obtained with TRILEGAL and Besançon models respectively for a field in the direction of NGC 2298, with a similar solid angle to that of the observed area around the cluster. The remarkable over-density observed in the bluer region of the observed CMD with $V > 24$ is generated by the presence of background galaxies in the wide-field photometry. In order to compare both synthetic models, we have selected the area in the CMD defined by $0.6 < B - R < 1.5$ and $21 < V < 23.5$ (over-plotted grey rectangle).

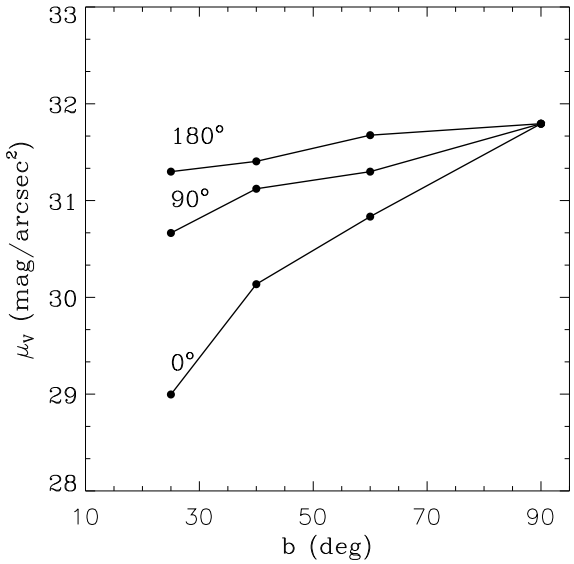

Figure 5.8: Limiting surface-brightness for three directions in the sky (ℓ = 0, 90 and 180°), defined by the star counts required to obtain a 5σ signal above TRILEGAL. As expected, faint substructures as tidal streams will be more easily detectable at higher values of b, far from the Galactic stellar components (disc, bulge).

be differentiated from the fore/background populations in the area around the Galactic centre ($\ell = 0°$, $b < 40°$) is brighter compared to the values obtained for the same stream in the Anticentre direction. These results indicate the areas where faint stellar substructures as the known tidal streams will be more easily detectable.

5.3.3 Finding stellar debris with a cross-correlation algorithm

Given that the detections (and their significances) derived from the synthetic CMDs might depend on the selection of the Milky Way model and the input parameters, we have also used an alternative approach to look for MS features of stellar streams based on the cross-correlation method described in Pila-Díez et al. (2014). This algorithm has been succesfully proven in the case of a photometric pencil-beam survey of the Sgr tidal stream using CFHT MegaCam deep data but lacking control fields adjacent to the target fields, which is the same situation of our GC survey. This method is based on an algorithm that takes a CMD as an input and looks across it for the over-density that best matches a template MS population. The template MS is built from the shape of an old, metal-

poor theoretical isochrone[1](Marigo et al. 2008; Girardi et al. 2010) matching the specific photometric system of the CMD. The width of this template MS is tailored to the photometric quality of the CMD by accounting for the increase in colour error with magnitude of a well defined stellar locus (particularly, the nearby M-dwarf stars at $2 < B - R < 3$). To each region of the MS template a weight based on the distance to the central region of the template is given so that - for each step of the cross-correlation - stars placed in the inner part of the template have a larger weight than stars at the edges of the template. This accounts for possible outliers and statistical contamination.

The algorithm returns two products: the first one is a binned density diagram in the colour-magnitude space recording the stellar density contained within the template MS for each iteration of the cross-correlation. The second one is the MS TO point coordinates (in the colour-magnitude space) for the best match (peak of the cross-correlation). We used these binned density diagrams to evaluate the quality of the detection by estimating the signal-to-noise of the cross-correlation procedure and used this last parameter to determine whether the best match actually represents a real halo feature. We define a positive detection when the S/N is larger than 5. In all cases with S/N>3, we can use the MS TO point magnitude to calculate the distance modulus and the heliocentric distance to the substructure (see below). For the templates in this work we have used two types of theoretical isochrones: one corresponding to the age and metallicity of each GC, which we use on both the corresponding GC and on the extratidal field at $r > r_{\rm bg}$ CMDs, and another one corresponding to possible subjacent streams, which we only use for the outer-region CMDs.

5.3.4 Distances to the underlying populations with isochrone fitting

Distances to the hypothetical tidal debris are fundamental to conclude if they are associated to the GCs or a background, unassociated tidal stream or Galactic substructure. Heliocentric distances were derived from the position of the MS-feature of the tidal debris in the CMD by fitting a reddening-corrected theoretical isochrone. First, the selected isochrone is shifted by varying the distance modulus in the range $12 < (m - M)_{\rm V} < 19$ with a step of $\delta(m - M)_{\rm V} = 0.2$. The χ^2 for each position was computed taking into account all the stars located in the MS feature (mainly populated by the possible stream stars and Galactic halo stellar component). The distance modulus value corresponding to the minimum χ^2 is then selected as initial input for an iterative procedure to obtain a more accurate estimate of the position of the isochrone. In this case, we analyzed the distance modulus range within a 10% above and below that value with a smaller step $\delta(\mathrm{m - M})_{\rm V} = 0.01$ ($\sim$150 pc). This fitting method has been tested using the CMD corresponding to the inner regions of the GCs, for which we used

[1]This isochrone and all the ones associated to the cross-correlation have been retrieved from the Padova Stellar Evolution database, available at http://stev.oapd.inaf.it/cmd.

the isochrones assuming previous estimates for their age t and [Fe/H] (Forbes & Bridges 2010; Harris 2010). Figure 5.9 shows the comparison between the $(m - M)_{\rm V}$ obtained for the 23 globulars and those listed in the Harris catalog. There is no evidence of systematic deviation from the 1:1 line, this is also confirmed by the obtained correlation coefficient ($r = 0.97$). This test confirms that it is possible to obtain the heliocentric distances for stellar remnants using our method and, more importantly, there are not systematic effects in our photometry, even though is based in observing campaigns from two different telescopes spread over ten years.

Because of the lack of a red-giant branch (RGB) feature associated to the detected tidal debris, it is not possible to obtain insights on their metallicity from our CMDs. This also prevents us from selecting the most suitable isochrone for each case. For this reason, we use only two different cases for our derivation of these distances: in the case of the remnants possibly associated to the Sgr stream (see Section 5.5.1), we used an isochrone based on Siegel et al. (2007) results, with an intermediate age of $t = 6\,$Gyr with [Fe/H] = -0.6. For the over-densities found around other clusters, we assume that they are dominated by an old stellar population similar to those of the typical Milky Way dSph galaxies (i.e. Ursa Minor or Draco). In these cases, an isochrone with $t = 12\,$Gyr and [Fe/H] = -1.5 is used for the fitting method described above. We have used the theoretical isochrones generated by Dotter et al. (2008b) in combination with the Galactic extinction maps from Schlegel et al. (1998) and the extinction coefficients from Schlafly & Finkbeiner (2011). Possible effects of spatial variations on the extinction over the FOV are expected to be smalle ($\Delta E(B-V) < 0.02$) even in the clusters at the lowest latitude included in our sample, and have been neglected. The resulting heliocentric distance for the possible tidal remnants detected in this study are given in Table 5.3.

In addition to these distance estimates, the MS TO point coordinates for the best match (i.e. peak of the cross-correlation) obtained from the algorithm described in Section 5.3.3 were used to calculate the distance modulus and the heliocentric distance to the substructures. The potential age and metallicity gradients of the subjacent streams and their effect on the distance calculation have been included in the uncertainties as discussed in Pila-Díez et al. (2014). The results of this method are given in Table 5.4.

5.4 Results

Figures from 5.10 to 5.15 show the calibrated CMDs for the GGs in our sample. For each cluster, we show the CMD for its central region (middle panel) and for those stars situated at a distance beyond $r_{\rm bg}$ from the cluster centre (right panel; with the exception of Pal 5, see below). In order to avoid crowding problems, we have included only a fraction of the central regions of the cluster confined between an arbitrary distance from the centre and the half-mass radius ($r_{\rm h}$), which generates the differences in limiting magnitude between the diagrams in some of the clusters (e.g. NGC 6229 and NGC 4590). The left panels display the

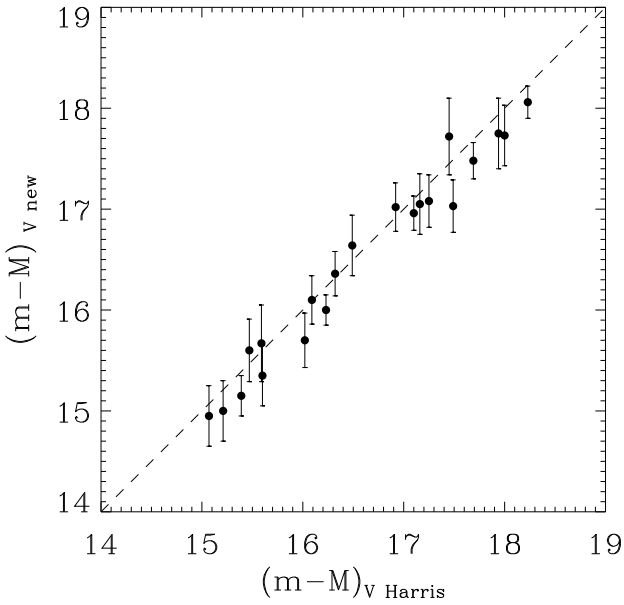

Figure 5.9: Comparison between the Harris (2010) distance modulii and the values derived using the isochrone fitting method described in Section 5.3.4. $(m-M)_{\rm V}$ and $(m-M)_{\rm VHarris}$ represent the distance modulus obtained for the GCs included in our sample and the one taken from the Harris catalog respectively. The dashed line indicates the 1:1 relation.

Table 5.3: Results from the isochrone fitting method described in Section 5.3.4. Areas observed, distances derived for the GCs and for the subjacent populations are given in the columns labeled with A_{bg}, d_{GC} and d_{bg} respectively. Significance of the detections S_T and S_B, with respect to TRILEGAL and Besançon respectively, are computed using the number of star counts in the observed CMD (N_{CMD}) and the counts for the same area of the diagrams obtained with the model considered here (N_T or N_B). The identity of the subjacent population is suggested in function of the projected position of the sample and the considered model. Clusters ordered by S_T.

Cluster	A_{bg} (deg^2)	d_{GC} (kpc)	d_{bg} (kpc)	N_{CMD}	N_T	N_B	S_T	S_B	Note
NGC 5634	0.21	25.7± 3.8	47.9 ± 4.7	190	36.2	50.1	10.2 ± 0.8	9.0 ± 0.9	Sgr
Whiting 1	0.31	25.4± 3.2	26.3 ± 3.3	181	35.2	20.3	10.0 ± 0.8	11.3 ± 0.7	Sgr
NGC 4147	0.23	21.6± 2.3	29.3 ± 4.9	254	95.7	88.2	8.5 ± 0.9	9.0 ± 0.9	Sgr
NGC 5053	0.17	13.2± 3.7	32.8 ± 5.3	86	10.0	29.4	7.8 ± 0.7	5.2 ± 0.9	Sgr
Pal 5	0.18	25.4± 2.9	52.8 ± 5.6	244	106.7	58.5	7.3 ± 0.9	10.7 ± 0.8	Sgr
			27.6 ± 3.8	108	24.6	34.2	7.2 ± 0.8	6.2 ± 0.9	Tail
NGC 7006	0.52	40.9± 2.1	22.3 ± 2.5	705	455.4	410.2	7.3 ± 1.0	8.8 ± 1.0	Her–Aq/?
NGC 7492	0.22	26.3± 2.1	22.0 ± 3.8	136	46.3	85.2	6.6 ± 0.9	3.4 ± 1.0	Sgr
NGC 1851	0.36	24.7± 2.0	11.9 ± 2.0	227	125.2	90.2	5.4 ± 1.0	7.7 ± 0.9	Mon?/GC Halo
NGC 1261	0.21	16.6± 2.0	14.9 ± 2.6	151	71.4	71.8	5.3 ± 1.0	5.3 ± 1.0	Tail?
NGC 5024	0.13	18.7± 2.0	37.7 ± 5.7	48	15.7	26.0	4.1 ± 0.9	2.6 ± 1.0	Sgr
NGC 7078	0.20	10.0± 1.7	14.4 ± 3.7	218	160.2	168.3	3.0 ± 1.0	2.5 ± 1.0	Her–Aq/?
NGC 1904	0.32	13.6± 2.1	15.4 ± 2.4	132	98.4	94.2	2.2 ± 1.0	2.5 ± 1.0	?/GC Halo
NGC 6229	0.24	35.0± 3.1	17.7 ± 3.2	98	71.9	82.2	2.0 ± 0.9	1.2 ± 0.9	Her–Aq/?

position of the stellar sources considered in our final photometric catalogs with respect to the position of the cluster centre. This provides a good reference for the sky area (in degrees; see Table 5.3) covered around each target in this work. The total area observed around each cluster was estimated taking into account the gaps between the chips at both instruments and the position of the cluster centre in the field.

The significance of the underlying populations by means of the comparison with a synthetic CMD from the TRILEGAL and Besançon Galactic models is shown in Table 5.3. The number of observed stars ($N_{\rm CMD}$) and the TRILEGAL and Besançon counts ($N_{\rm T}$ and $N_{\rm B}$ respectively) are used to calculate $S_{\rm T}$ and $S_{\rm B}$ using Equation 5.3. In Table 5.3 we show the derived heliocentric distances for their $r > r_{\rm bg}$ populations. Given that the S values depend clearly on the synthetic Milky Way model and the input parameters used (Table 5.3), our positive detections are compared with the results obtained from the application of the cross-correlation method to the region defined by $0.0 < B - R < 1.6$ and $18.0 < V < 24.0$ in the $r > r_{\rm bg}$ CMDs. According to these results, we group the clusters in the following categories:

- Group A: Clusters for which neither the comparison with Galactic models nor the cross-correlations return significant detections ($S < 5$; $S/N < 5$). These CMDs correspond to the clusters AM4, NGC1904, NGC 2298, NGC4590, NGC5024, NGC5272, NGC5466, NGC 5694, NGC 5824, NGC6229, NGC 6864, NGC 7078, Pal 15 and Rup 106. We refer to this group as "no detections".

- Group B: Clusters for which an overdensity with $S > 5$ is detected with respect one of the adopted reference Galactic field models and the CMD cross-correlation provides a good match with $S/N > 5$. The only cluster in this group is NGC7492. We refer to this group as "uncertain" detections.

- Group C: Clusters for which an overdensity with $S > 5$ using both reference Galactic field models is detected but the CMD cross-correlation provides an inconclusive result. The CMDs in this group correspond to NGC5053 and NGC7006. We refer to this group as "possible" detections.

- Group D: Clusters for which an overdensity with $S > 5$ using both reference Galactic field models is detected and the CMD cross-correlation identifies a distinct MS with $S/N > 5$ and pins its TO point. The CMDs in this group correspond to NGC 1261, NGC 1851, NGC 4147, NGC 5634, Pal 5 (twice) and Whithing 1. We refer to this group as "probable" detections. Their density diagrams are shown in Figure 5.16.

The distance moduli and heliocentric distances to the structures belonging to group D are calculated using the cross-correlation algorithm and the two possible isochrones mentioned above (either the one from the nearby GC or the one from

Table 5.4: Cross-correlation results for every field (both inner and outer). For every field we indicate whether there is a detection (D) or not (B), or if the field presents any problem for the method (A and C). For all the inner cases and the outer D cases, we include the cross-correlation MS TO point in the V band. For these fields we also provide the distance modulus and heliocentric distance (in kpc) as derived from two different theoretical isochrones: one representing the stellar population of the nearby GC ($d_{\mathrm{GC-iso}}$) and the other one representing that one of the Sgr stream ($d_{\mathrm{Sgr-iso}}$).

Cluster	Field	Group	S/N	$\mathrm{TO_V}$	$(m-M)_{\mathrm{V\ GC-iso}}$	$d_{\mathrm{GC-iso}}$	$(m-M)_{\mathrm{V\ Sgr-iso}}$	$d_{\mathrm{Sgr-iso}}$
am4	in		5.4	21.0	17.2	28 ± 2	17.2	28 ± 2
am4	out	A						
ngc1261	in		4.4	19.8	15.9	15 ± 1	16.0	16 ± 1
ngc1261	out	D	6.9	20.0	16.1	16 ± 2	16.2	18 ± 2
ngc1851	in		3.9	19.4	15.5	13 ± 1	15.6	13 ± 1
ngc1851	out	D	7.3	19.0	15.1	11 ± 1	15.2	11 ± 1
ngc1904	in		4.0	19.8	15.9	15 ± 1	16.0	16 ± 1
ngc1904	out	A	4.4	20.2	16.3	18 ± 2	16.4	19 ± 2
ngc2298	in		6.4	19.5	15.5	13 ± 1	15.7	14 ± 1
ngc2298	out	A						
ngc4147	in		6.7	20.5	16.6	21 ± 1	16.7	22 ± 1
ngc4147	out	D	5.0	21.9	18.0	41 ± 6	18.1	42 ± 6
ngc4590	in		4.5	19.1	15.4	12 ± 1	15.3	12 ± 1
ngc4590	out	A						
ngc5024	in		5.4	20.4	16.5	20 ± 1	16.6	21 ± 1
ngc5024	out	A						
ngc5053	in		4.9	19.9	16.1	17 ± 1	16.1	17 ± 1
ngc5053	out	C						
ngc5272	in		6.0	18.1	14.2	6.8 ± 0.3	14.3	7.3 ± 0.3
ngc5272	out	A						
ngc5466	in		5.9	19.9	15.9	15 ± 1	16.1	17 ± 1
ngc5466	out	A						
ngc5634	in		4.3	21.1	17.2	28 ± 1	17.3	29 ± 1
ngc5634	out	D	6.5	22.4	18.5	51 ± 9	18.6	53 ± 10
ngc5694	in		5.0	22.1	18.1	42 ± 2	18.3	46 ± 2
ngc5694	out	A						
ngc5824	in		4.9	22.1	18.1	42 ± 2	18.3	46 ± 2
ngc5824	out	A						
ngc6229	in		5.3	21.5	17.5	32 ± 2	17.7	35 ± 2
ngc6229	out	A						
ngc6864	in		4.7	20.9	17.0	26 ± 1	17.1	27 ± 1
ngc6864	out	A						
ngc7006	in		4.8	22.2	18.3	45 ± 2	18.4	48 ± 2
ngc7006	out	C						
ngc7078	in		4.1	19.8	15.9	16 ± 1	16.0	16 ± 1
ngc7078	out	A						
ngc7492	in		4.7	20.5	16.6	21 ± 1	16.7	22 ± 1
ngc7492	out	B	5.4	20.2	16.3	18 ± 2	16.4	19 ± 2
pal15	in							
pal15	out	A						
pal5	in		6.4	20.8	17.0	25 ± 1	17.0	25 ± 1
pal5	out	D	5.0	22.6	18.8	58 ± 6	18.8	58 ± 6
pal5	out	D	6.1	20.8	17.0	25 ± 2	17.0	25 ± 2
rup106	in		4.7	21.0	17.2	27 ± 1	17.2	28 ± 1
rup106	out	A						
whit1	in		5.4	20.8	17.3	29 ± 3	17.0	25 ± 2
whit1	out	D	5.2	20.5	17.0	26 ± 2	16.7	22 ± 1

the Sgr stream). The derived distances (Table 5.4) are consistent with those obtained using the isochrone fitting method given in Sec. 3.4, without any evidence of systematic offset or trend. We thus conclude that the cross-correlation method independently confirms (within the uncertainties) the distance measurements for the GCs classified as group D.

5.5 Discussion

5.5.1 Overdensities associated with the Sagittarius tidal stream

The stellar debris around clusters possibly associated with the Sgr tidal stream are, in general, the easiest cases to identify since the position and distance along the stream is well known from wide-sky surveys (Majewski et al. 2003; Belokurov et al. 2006b; Koposov et al. 2012) or numerous N-body simulations (Law & Majewski 2010b; Peñarrubia et al. 2010, hereafter P10). To check the possible presence of Sgr tidal debris in our sample, we overplot the position and distances of our sample to the Sgr tidal stream model presented by P10 in the (RA, Dec) and $(\ell, d_{\odot})$ planes (Figure 5.17). We find that 13 GCs of our sample lie within the projected position of the stream: Whiting 1, NGC 4147, NGC 4590, NGC 5024, NGC 5053, NGC 5272, AM 4, NGC 5466, NGC 5634, NGC 5694, Pal 5, NGC 6864 and NGC 7492. In addition to this comparison with theoretical models, we compare the projected position of these clusters with the MS star density map of this structure from the SDSS by Koposov et al. (2012). This shows that NGC 5466 and NGC 5272 are out of the projected path of the stream, which is consistent with our negative detections of tidal debris around these clusters. This could be also the case for NGC 6864, NGC 5694, NGC 4590 and AM 4 (see below).

Our survey around these Sgr stream GC candidates reveals the clear presence of "probable" tidal debris from this stream around four of these clusters (Whiting 1, NGC 4147, NGC 5634 and Pal 5; see CMDs in Figure 5.18) plus a "possible" debris around NGC 5053 and an "uncertain" debris around NGC 7492.

One of the most significant ($S_T, S_B > 10$) detections is unveiled in the area observed around the low-mass cluster Whiting 1, which was also suggested as member of the Sgr GC system by Carraro et al. (2007). The break in the radial stellar distribution found at ~ 6 arcmin (Carraro et al. 2007) suggests that this low-density cluster is currently going through a disruption process due to the forces exerted by the Milky Way. However, it seems unlikely that the highly contrasted MS discovered in the area close to the cluster ($B - R \sim 1$, $20.5 < V < 23$) shown in Figure 5.10, lacking of any collimated spatial distribution, was generated by stars that have (or are close to) left Whiting 1. We identify the subjacent system as the trailing arm of the Sgr tidal strem and the position of the cluster relative to the stellar over-densities associated with that halo substructure supports that scenario (Koposov et al. 2012).

The isochrone fitting shows that Sgr and Whiting 1 are spatially coincident, as also suggested by the cross-correlation results in Table 5.4. The confirmation of the association of such a young GC (6.5 Gyr; Carraro et al. 2007) will help to study

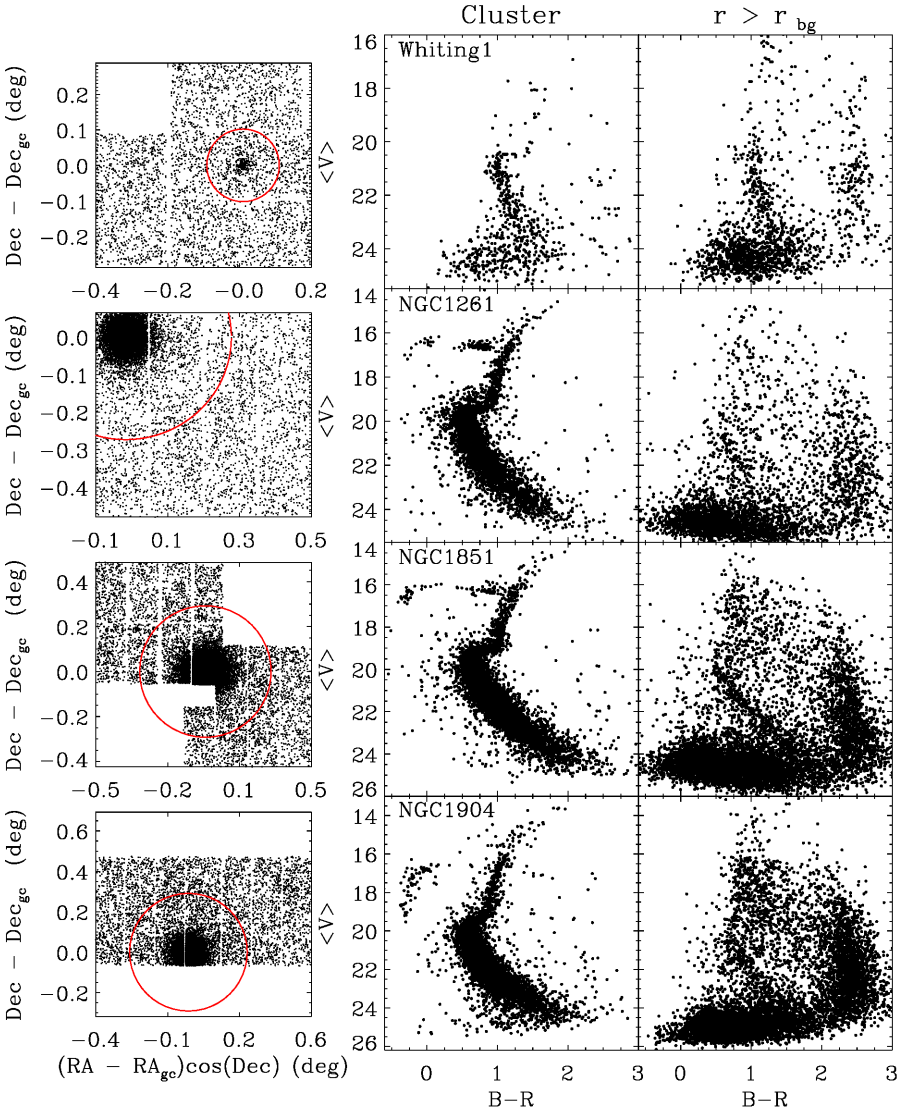

Figure 5.10: CMDs corresponding to the clusters Whiting 1, NGC 1261, NGC 1851 and NGC 1904 (middle column) and to those objects beyond $r_{\rm bg}$ from the cluster centre (right column). A map showing the distribution of the stars in the catalog with respect to the cluster centre is also included (left), where $r_{\rm bg}$ is indicated by a red line.

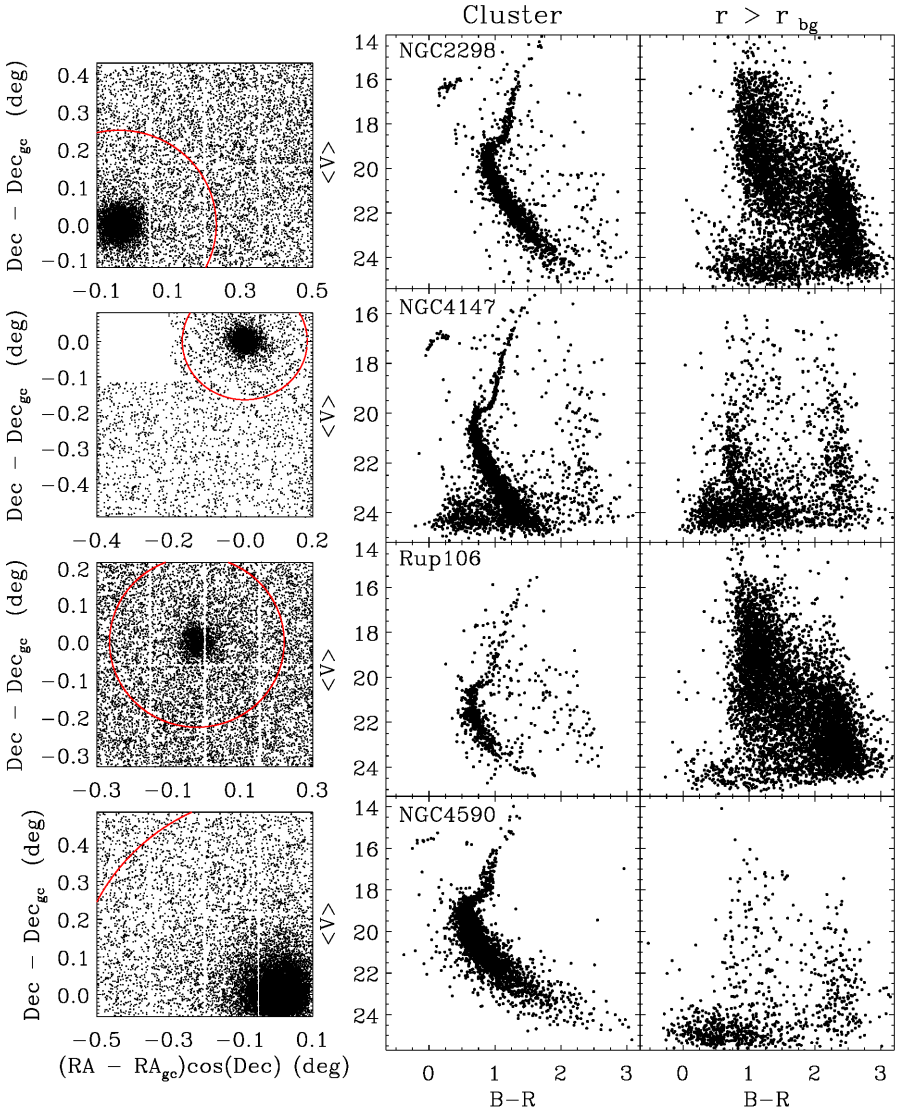

Figure 5.11: CMDs corresponding to the clusters NGC 2998, NGC 4147, Rup 106 and NGC 4590 (middle column) and to those objects beyond $r_{\rm bg}$ from the cluster centre (right column). A map showing the distribution of the stars in the catalog with respect to the cluster centre is also included (left), where $r_{\rm bg}$ is indicated by a red line.

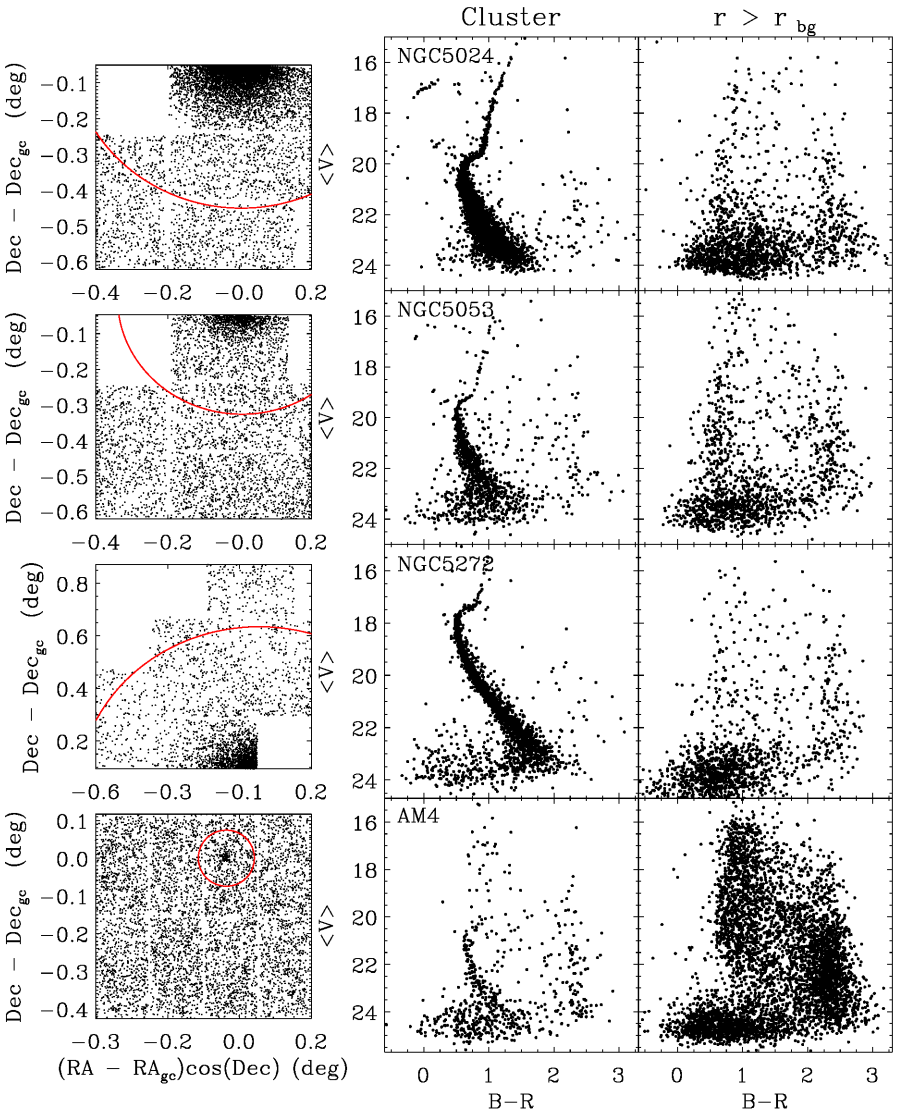

Figure 5.12: CMDs corresponding to the clusters NGC 5024, NGC 5053, NGC 5272 and AM 4 (middle column) and to those objects beyond $r_{\rm bg}$ from the cluster centre (right column). A map showing the distribution of the stars in the catalog with respect to the cluster centre is also included (left), where $r_{\rm bg}$ is indicated by a red line.

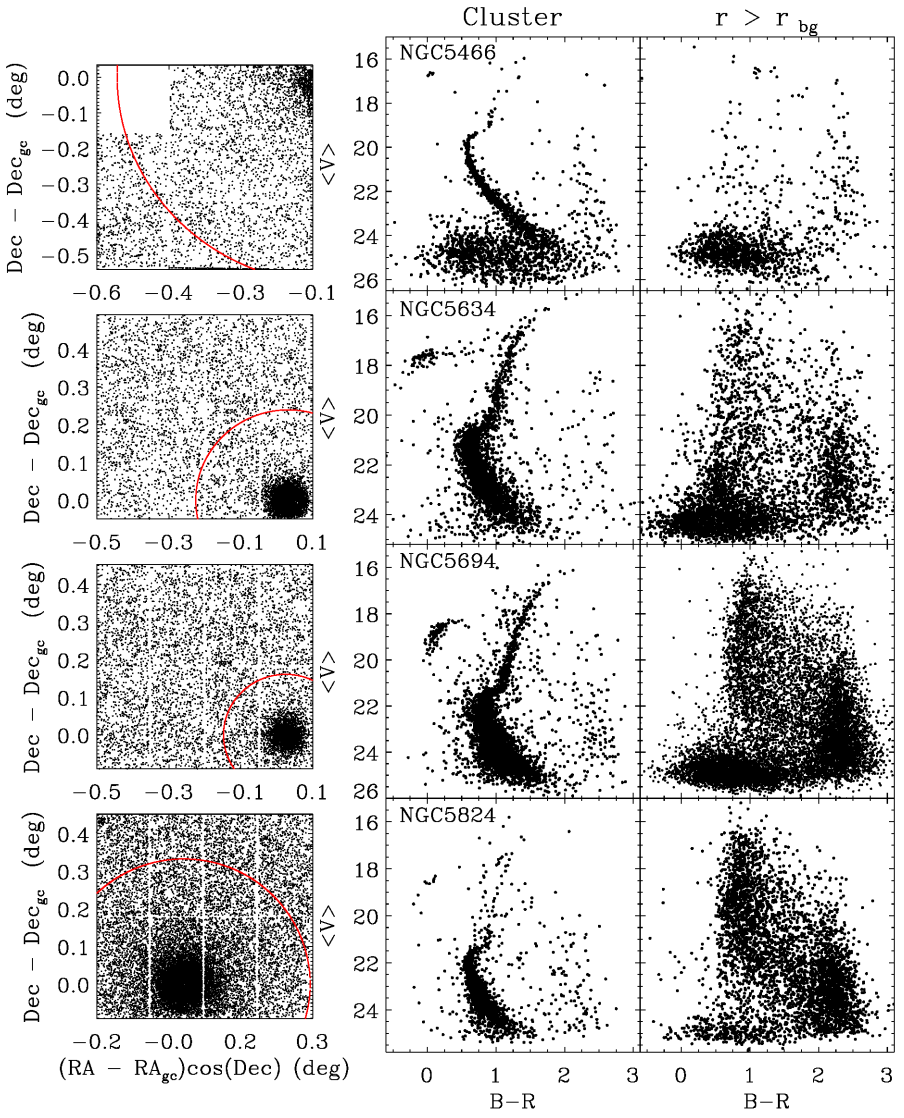

Figure 5.13: CMDs corresponding to the clusters NGC 5466, NGC 5634, NGC 5694 and NGC 5824 (middle column) and to those objects beyond $r_{\rm bg}$ from the cluster centre (right column). A map showing the distribution of the stars in the catalog with respect to the cluster centre is also included (left), where $r_{\rm bg}$ is indicated by a red line.

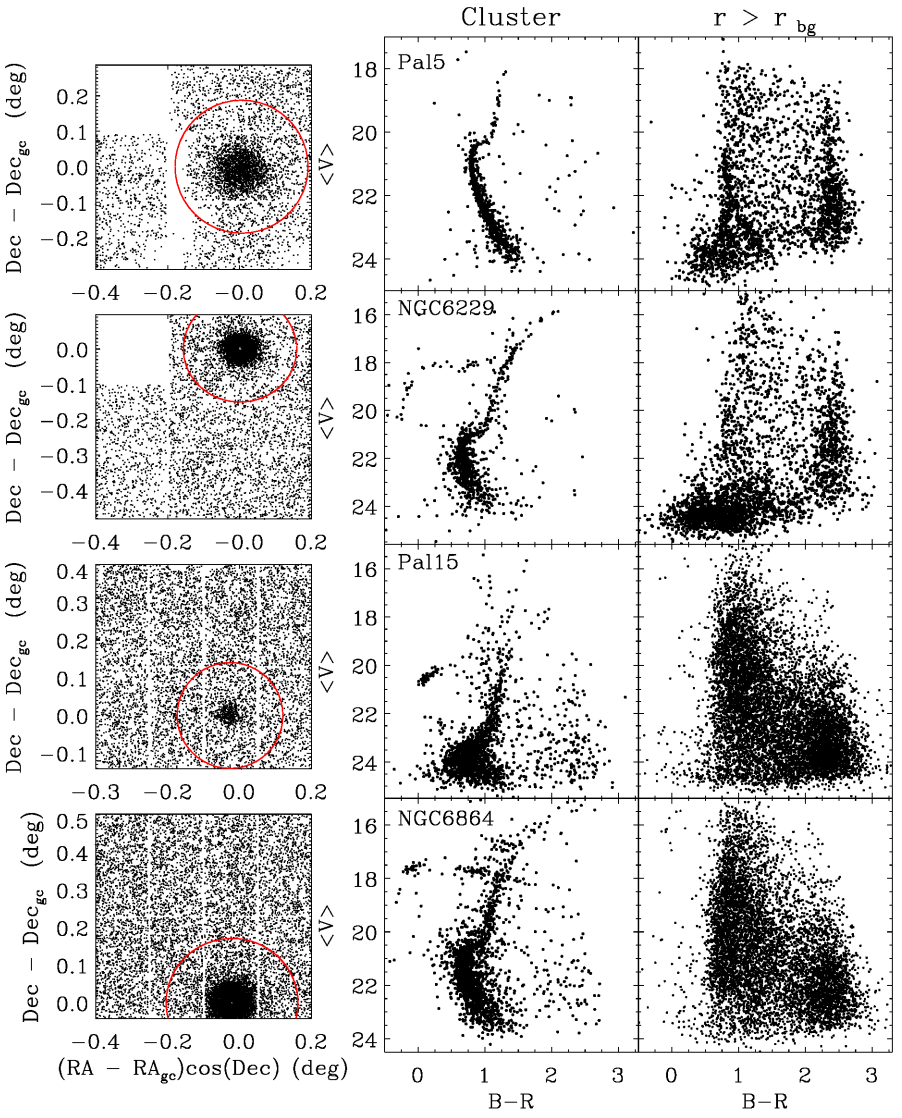

Figure 5.14: CMDs corresponding to the clusters Pal 5, NGC 6229, Pal 15 and NGC 6864 (middle column) and to those objects beyond $r_{\rm bg}$ from the cluster centre (right column). A map showing the distribution of the stars in the catalog with respect to the cluster centre is also included (left), where $r_{\rm bg}$ is indicated by a red line.

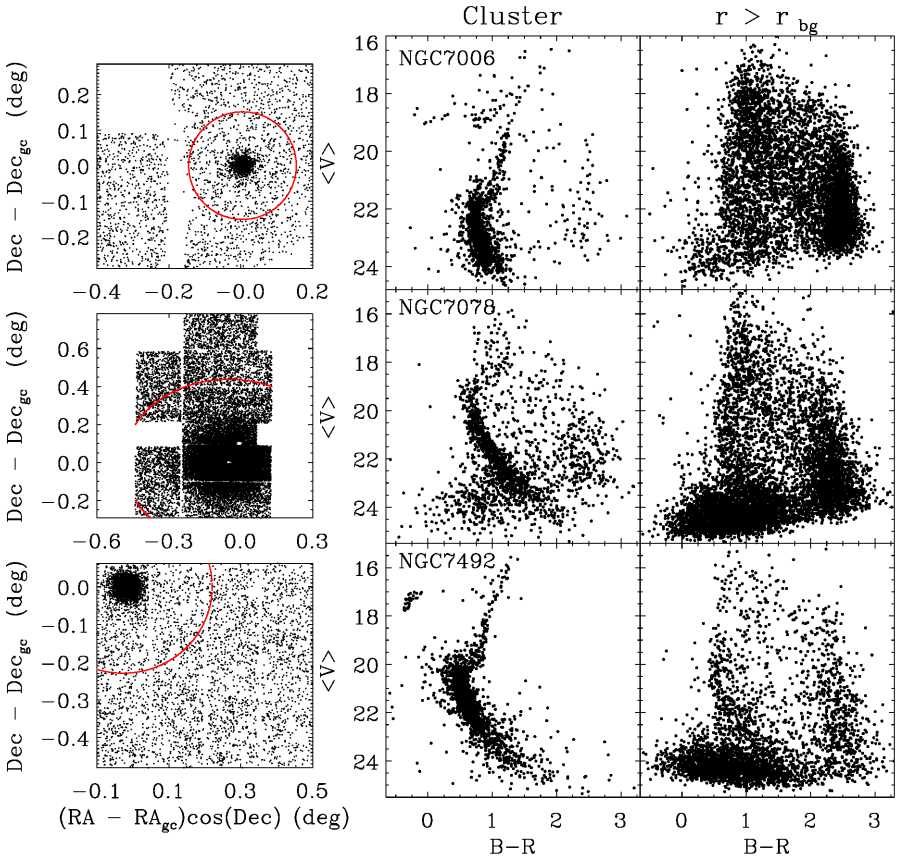

Figure 5.15: CMDs corresponding to the clusters NGC 7006, NGC 7078 and NGC 7492 (middle column) and to those objects beyond $r_{\rm bg}$ from the cluster centre (right column). A map showing the distribution of the stars in the catalog with respect to the cluster centre is also included (left). Note that in the case of NGC 7006, only one of the pointings has been included in that map, where $r_{\rm bg}$ is indicated by a red line.

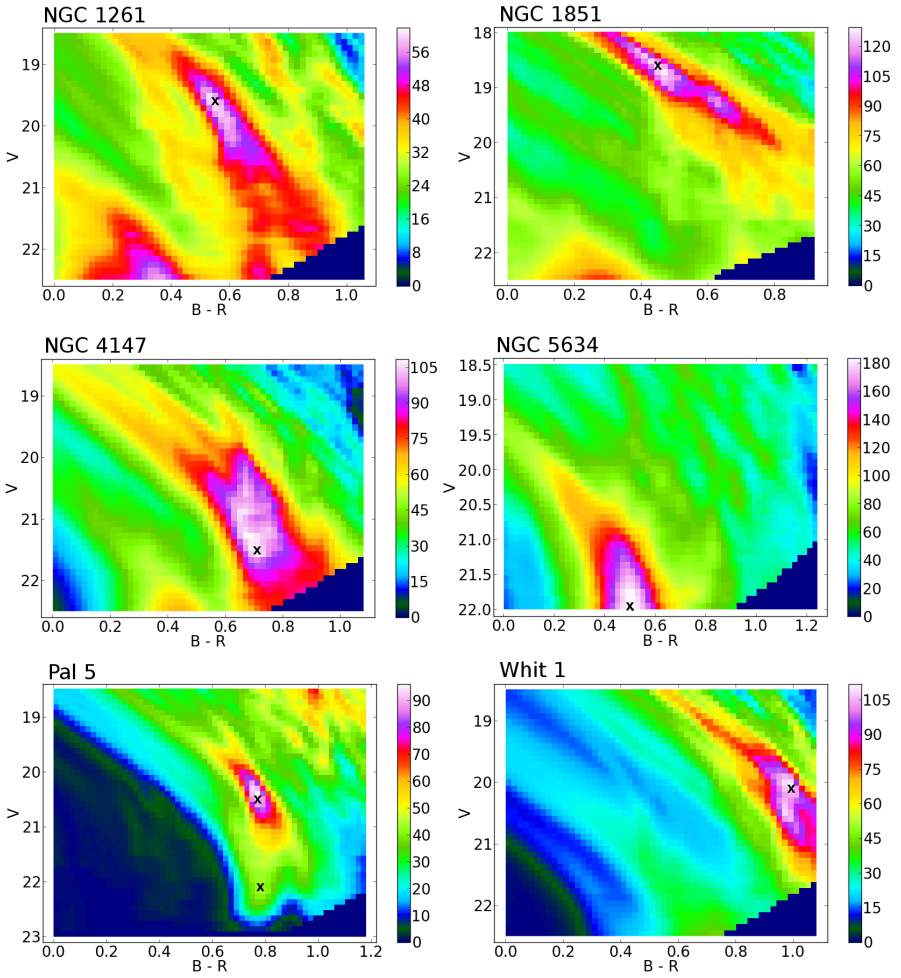

Figure 5.16: Density diagrams resulting from cross-correlating the CMDs of the outer regions with the MS template. From left to right and top to bottom: NGC1261, NGC1851, NGC4147, NGC5634, Pal 5 (twice) and Whiting 1.

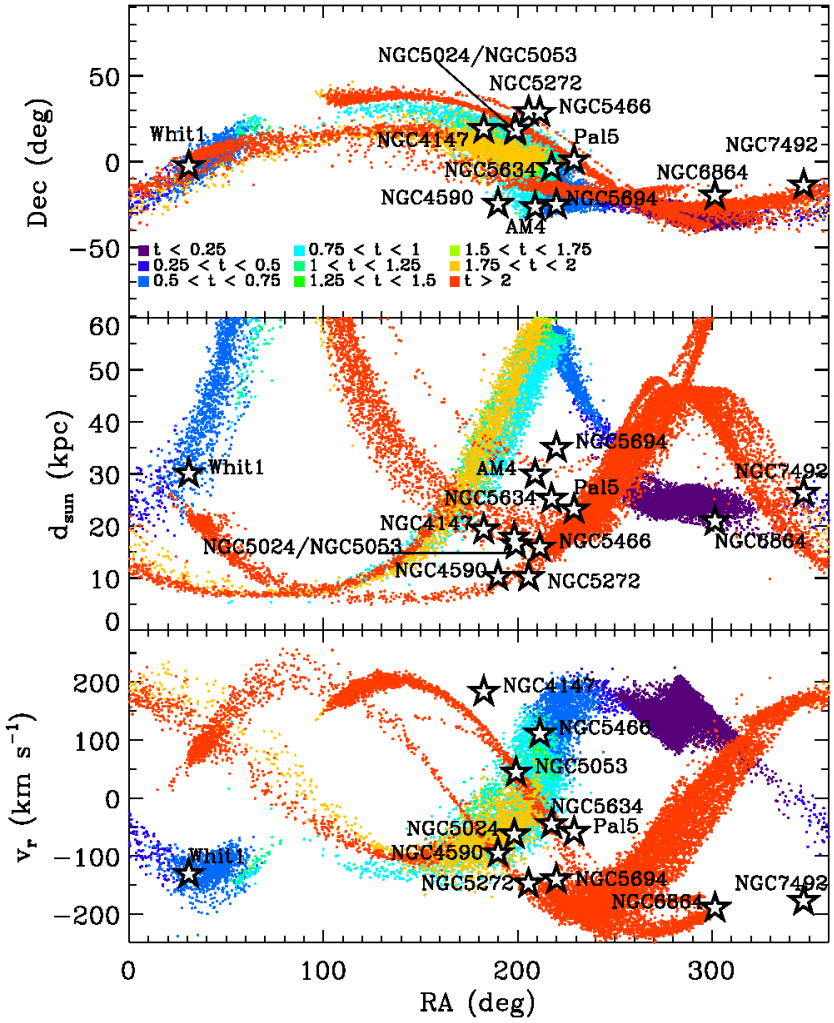

Figure 5.17: The Sgr tidal stream as presented in the model by P10. The upper panel shows the predicted orbit of the stream in the sky where the colour indicate different accretion times for the particles in ranges of 0.25 Gyr long. The middle and bottom panels show the heliocentric distance and radial velocity distribution of the stream, using the same colour scheme. The position and radial velocity of the globulars in our sample are over-plotted as stars. Only the fraction of the substructure with $d_{\odot} < 60$ kpc has been considered.

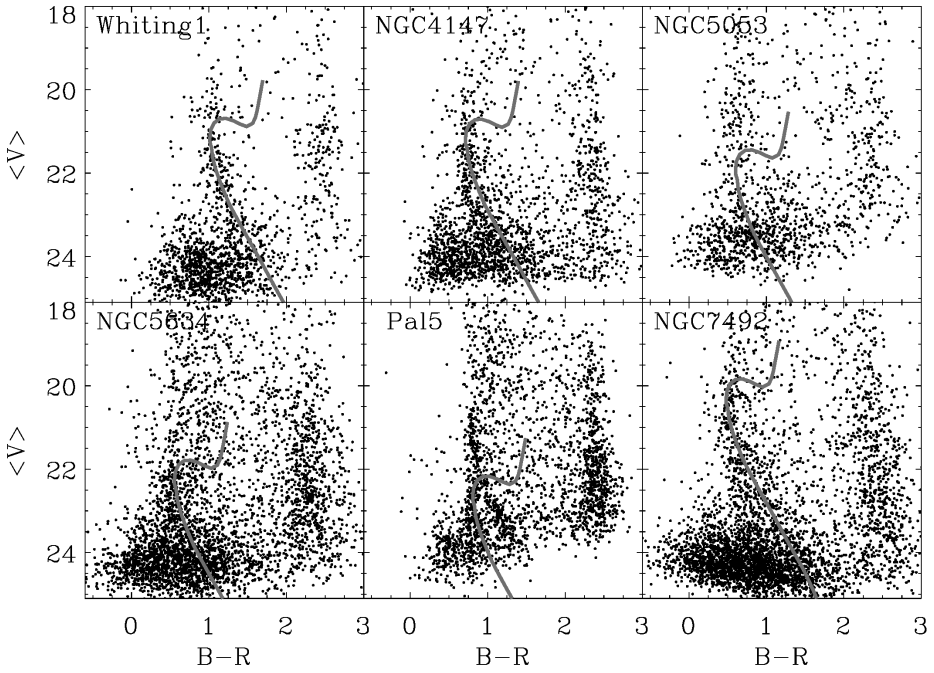

Figure 5.18: CMDs for the surrounding area of the GCs possibly associated with the Sgr tidal stream, with stellar over-densities that stand out in the comparison with the synthetic diagrams. The Sgr isochrone corresponding to the radial distance derived is over-plotted.

the GC formation process in Sgr, given that Whiting 1 might be the youngest GC among the clusters already associated with that dSph (~ 1 Gyr younger than the intermediate–age GCs Arp 2, Ter 7 and Pal 12, already associated to Sgr). This would indicate that Sgr was able to form GCs during a period of 6 Gyr as pointed by Carraro et al. (2007).

NGC 5634 is one of the closest clusters to the plane that contains the orbit of the Sgr dSph (L10) and stream stars were identified by Majewski et al. (2003) in that line-of-sight. Our photometry shows for the first time a CMD morphology compatible with that of the Sgr stream in the surroundings of this cluster. It however does not reveal any underlying population at a similar distance of this cluster. A more important contribution in the background is detected, at a distance nearly twice the distance to NGC 5634, as confirmed by both distance determination methods. On the basis of the P10 model, we identify that system in the background as a distant section of the leading arm of the Sgr tidal stream.

The CMD of Pal 5 presents the most complex morphology in our survey, displaying two MS-like features at different distances as shown in Figure 5.18. The first lies is a high significance stellar population in the background of Pal 5 at a similar distance of the cluster. These stars are likely cluster members populating the well-studied massive tidal tails emerging from this cluster (Odenkirchen et al. 2001; Rockosi et al. 2002; Grillmair & Dionatos 2006a). A second and significant ($S \sim 8$) MS is detected below the feature associated to the tidal tails (see Fig. 12 in Pila-Díez et al. 2014) at a radial distance compatible with that of the Sgr tidal stream according to P10. Interestingly, Sbordone et al. (2005) derived α-element abundances for Pal 5, resembling those obtained for M 54 and Ter 7, members of the Sgr GC system.

Bellazzini et al. (2003) argued for the association of NGC 4147 with the Sgr stream from its radial velocity and the detection of M giant Sgr stars around this cluster. The detection of a MS feature from the Sgr stream stellar population around NGC 4147 in our pencil-beam survey was already reported in Martínez-Delgado et al. (2004a), before the mapping of this structure with large-scale surveys (e.g. Majewski et al. 2003; Belokurov et al. 2006b; Koposov et al. 2012). We detect an underlying stellar population likely associated to that halo substructure at $d_{\odot} \sim 35$ kpc, separated from the GC along our line-of-sight by ~ 15 kpc, in agreement with the position of the leading arm predicted by P10. Our results indicate that this cluster is not immersed in the Sgr tidal stream, as also pointed out in Martínez-Delgado et al. (2004a), where the integrals of motions of both systems were analyzed. SDSS mapping has also showed that the path of the stream crosses the surroundings of NGC 5024 and NGC 5053, which are in the vicinity of NGC 4147 in projected position (see Koposov et al. 2012).

Around NGC 5053 (classified in the group C) we have found an over-density in its background CMD suggesting a subjacent population at ~ 40 kpc, compatible with the radial distances predicted by P10 for the Sgr leading arms on that direction of the sky. The significance for the over-density in NGC 5024 is $S < 5$. However, the cross-correlation method returns unconclusive or ambiguous detec-

tions in the case of both globulars, likely produced by the presence of blended populations in the diagrams, with a second MS possibly corresponding to a more distant wrap of Sgr with a low S/N. From these globulars, only NGC 5053 is presented by L10 as a genuine candidate to belong to the Sgr GC system.

NGC 7492 is the only cluster of our sample for which an "uncertain" detection of an underlying debris (group B) has been found, and it is one of the globulars with low probability of belonging to the Sgr GC system according to L10. We identified a subjacent MS feature at a distance compatible with that of the cluster, which is not predicted in the synthetic TRILEGAL CMDs, while the significance of such a feature drops below the adopted treshold when the Besançon model is adopted. With our photometry only, it is not possible to address the question of whether this detection is real or associated to tidal tails originating from the cluster. However, in the radial profile obtained for this cluster (see Carballo-Bello et al. 2012), the stellar density beyond $r_{\rm bg}$ (~ 14 arcmin) suggests the presence of a homogeneously distributed population. This suggests that the eventual underlying population is associated to a different system in the background of NGC 7492. Figure 5.17 shows that the projected position and distance of the most recent accreted fraction of the Sgr stream trailing arm ($t_{\rm accr} < 0.25$ Gyr) is compatible with the position of this globular. Interestingly, the region around this cluster falls in a sky area without SDSS data (see Figure 5.19), but with evidence of Sgr stars in its vicinity, which strenghtens the hypothesis that this GC is embedded in the Sgr stream.

The negative detections in the surroundings of the other candidates prevent us from obtaining a final conclusion about the possible association of those clusters with the Sgr tidal stream, within our surface-brightness detection limits. Among them, only AM 4 has been suggested as member of the Sgr GC system by Carraro (2009) but, according to the background CMD obtained, there is no evidence of a subjacent stellar population associated to that stream. These negative detections, even in cases where the projected positions are favouring the detection of Sgr stream stars spatially coincident with the globulars (e.g. NGC 5053 or NGC 5634), might be used to establish the limitations of our photometric survey. Indeed, the absence of tidal remnants might be related to the evolution of the Sgr dSph and its interaction with the Milky Way. According to the model of P10, while Whiting 1 and NGC 7492 are spatially coincident with the Sgr stars accreted in the last 0.75 Gyr, NGC 5053, NGC 5634 and Pal 5 are surrounded by the material accreted from the satellite > 2 Gyr ago. This is a consequence of the fact that sections of the stream generated a long time ago are more dispersed, with a lower surface-brightness, and only the most recent arms of the Sgr tidal stream could be detected by our survey . This scenario is also valid for Pal 12, a cluster previously associated to Sgr by Martínez-Delgado et al. (2002), which in the context of the P10 model seems to be associated with the section of the stream accreted in the last 0.75 Gyr.

In the bottom panel of Figure 5.17 we compare the predicted radial velocity of the stream with those values measured for the clusters in our sample (Harris

2010). The globulars that are kinematically compatible and coincident with the position of the P10 tidal stream are Whiting 1, NGC 5053, NGC 5634 and Pal 5 (suggested as members of the Sgr GC system by L10). On the other hand, there is a difference of $\Delta v_{\rm r} \sim 100\,{\rm km\,s^{-1}}$ in the case of NGC 7492. So, for this stellar system, cluster and stream seem to be independent systems, although the orbit and structure of the Sgr stream in the southern sky are not well constrained because of the lack of a deep full-sky photometric database as the one available in the northern hemisphere (see discussion in L10, P10). Further follow-up spectroscopy is required to investigate the nature of the stellar population discovered around NGC 7492.

5.5.2 Other over-densities

The analysis of the CMDs corresponding to the GCs not associated with Sgr suggests the presence of MS features likely associated with subjacent stellar populations in three of them: NGC1261, NGC1851 and NGC7006. In this section, we discuss the possible origin of these tentative remnants and their possible association with other known over-densities or stellar streams already reported in the Milky Way.

An extended stellar over-density around NGC 1851?

One of the most conspicuous over-density of our survey, not associated with the Sgr stream, was detected around NGC 1851, first discovered by Olszewski et al. (2009), who interpreted this featuare as an *extended halo* surrounding this cluster up to distances of 75 arcmin ($\sim 6.5 r_{\rm t}$) from the cluster centre, and independently reported by (Carballo-Bello & Martínez-Delgado 2010).

NGC 1851 is one of the most interesting candidates in our sample because of its multiple stellar populations (Milone et al. 2008; Han et al. 2009) and the well-studied star-to-star abundance variations (e.g. Milone et al. 2009; Zoccali et al. 2009; Carretta et al. 2010, 2011; Campbell et al. 2012; Carretta et al. 2012), which suggest a scenario in which this cluster is the result of the merging of two previous GCs, formed in the nucleus of an accreted dwarf galaxy (Carretta et al. 2010; Bekki & Yong 2012). This cluster is member of a group of GCs formed by NGC 1851, NGC 1904, NGC 2298 and NGC 2808, which seems to be confined in a *sphere* with a radius of 6 kpc. That spatial distribution resembles that of M 54, Terzan 7, Terzan 8 and Arp2, globulars found in the main body of the Sgr dSph (Bellazzini et al. 2004; Martin et al. 2004). In addition, all 4 clusters show extended HB morphologies in their CMDs, feature that has been suggested as an indicator of an extra-Galactic origin in GCs (Lee et al. 2007).

Figure 5.10 shows the presence of the prominent MS population in the surroundings of this cluster, which is the same reported by Olszewski et al. (2009). This feature is not predicted by the TRILEGAL or Besançon models and it is also detected when the cross-correlation method is used (Table 5.4) at a similar heliocentric distance than the cluster. Using low resolution spectra for a sample of 107 stars selected from the same photometry presented in this work, Sollima

et al. (2012) detected a unexpected distinct stellar component with a radial velocity distribution that cannot be associated neither with the Galactic velocity field nor NGC 1851 outliers, with a mean difference with respect to those components of $\Delta v_{\rm r} \sim 150$ km s^{-1} and $\Delta v_{\rm r} \sim 200$ km s^{-1}, respectively. These authors discuss the possible association of this feature with the Monoceros ring, showing that the observed velocity distribution and the prediction made by the P05 model for that ring-like structure are slightly different, although not completely inconsistent given the uncertainties in the adopted Galactic potential. However, a recent spectroscopic analysis by Marino et al. (2014) analysed a set of medium-resolution spectra for a sample of stars in the outer halo of NGC 1851 reporting the lack of any significant over-density of stars at the velocity of such supposed stream. Summarizing, with the present dataset it is not clear if the detected over-density is linked to the precence of an extended halo of cluster member stars (as suggested by Olszewski et al. 2009) or to a subjacent stream (possibly the Monoceros ring). Deep data extending over a wider FOV are needed to distinguish between these two hypotheses.

NGC 7006

NGC 7006 is a cluster slightly younger than other similar clusters in the inner Galaxy (Dotter et al. 2011). In addition, this GC is one of the most energetic clusters in the Milky Way with a very eccentric orbit (Dinescu et al. 2001), suggesting and extra-Galactic origin for that system. Figure 5.15 show the presence of a significant MS feature in the outer region of NGC 7006 (first reported in Martínez-Delgado et al. 2004a). Since our cross-correlation method fails to detect these features due to the crowding of the fields (this cluster is classified in the group C), our distance estimates are only based on isochrone fitting (Table 5.3). Our results show that the hypothetic subjacent stellar population is at different distance from the cluster. In particular, we derived a difference in distance of $\sim$ 8 kpc for this possible tidal debris from the main body of NGC 7006. However, an inspection of the CMD of this cluster (Figure 5.15) shows that the MS TO of this feature is severely affected by the presence of bright Milky Way disc stars at $V \sim$ 20–21, making the estimate of its position very uncertain. Therefore, we believe that this population lies at a distance $d_{\odot} = 15 - 20$ kpc.

Figure 5.19 shows a stellar density map of MS-stars in a region of the sky from the SDSS photometric database, which includes both NGC7006 and NGC7078 (marked as open circles). These globulars seem to be inmersed in a region of high density of halo stars, that extends up to Galactic latitudes $b \sim -40°$ (see also Deason et al. 2014) and that might be the best explanation for the presence of this feature in the CMD of NGC7006. However, an accurate model for the shape of the stellar halo is needed to confirm this possibility.

An alternative scenario might be the presence of the southern component of the Hercules–Aquila over-density in the positions of this cluster. Recent results by Simion et al. (2014) supports the presence of a prominent over-density of RR Lyrae stars associated to this vast over-density in this region of the sky, with a distance

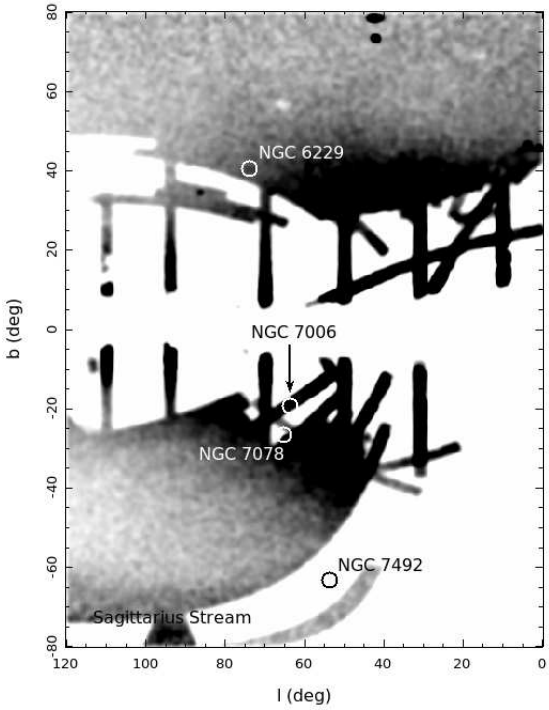

Figure 5.19: Density maps generated from SDSS data of the sky area where the GCs NGC 6229, NGC 7006, NGC 7078 and NGC 7492 are located. The huge stellar overdensity observed might be associated whether with the Hercules-Aquila cloud (Belokurov et al. 2007a; Simion et al. 2014) or with the region of higher density of halo stars reported by Deason et al. (2014). Note the presence of the Sgr stream in the bottom left corner of the map.

range of $10 < d_{\odot} < 25$ kpc (see their Fig. 9), strengthing the hypothesis of its origin from the tidal disruption of an ancient dwarf galaxy. That distance range is compatible with the one derived from our CMDs and suggests that NGC 7006 might be well embedded in (and possibly associated to) this giant cloud of debris. Interestingly, Simion et al. (2014) also found that the Hercules–Aquila cloud is barely visible as a RR Lyrae over-density in the northern hemisphere, suggesting that this cloud is possibly not symmetric with respect to the Galactic plane. This is consistent with the low significance overdensity ($S < 2.5$) of this component in the surroundings of NGC 6229 (see Figure 5.14).

NGC 1261

NGC 1261, lies in a projected position aligned with two other massive GCs showing an extended-HB morphology in their CMDs, NGC 1851 and NGC 1904. Around this cluster we have unveiled a stellar population (see Figure 5.10) that stands out significantly when the background diagram is compared with the ones generated with the considered Galactic models and it is also apparent in the results obtained through the cross-correlation method (see Table 5.4). The radial distance to the underlying component is similar to that of the cluster, suggesting that either it is composed of cluster members or of an unknown stellar population. The possible relation with the group of clusters described in Section 5.5.2 encourages to explore the area between NGC 1261 and those GCs.

5.5.3 Negative detections

There are no signatures of the presence of significant subjacent populations around the remaining candidates (AM4, NGC1904, NGC 2298, NGC4590, NGC5024, NGC5272, NGC5466, NGC 5694, NGC 5824, NGC6229, NGC 6864, NGC 7078, Pal 15 and Rup 106) as we find no evidence of distinct stellar population concentrated at a specific distance within the probed colour-magnitude range using both the cross-correlation and the isochrone fitting methods. The photometric non-detection of tidal debris around the halo GCs in this study is an important result to consider in the context of hierarchical stellar halo assembly theories. Whether or not such non-detections can rule out an accretion origin for these GCs (and a portion of the Milky Way stellar halo) depends on two main factors: 1) how massive were the progenitor dwarf galaxies these GCs were accreted with, and 2) when were these dwarf galaxies and their GCs accreted into the Milky Way? Indeed, GCs hosted in low luminosity dwarfs which were accreted early, may show minimal associated stellar debris when observed at present.

5.6 Conclusions

We have presented the wide-field photometry of 23 Galactic GCs in the Galactocentric distance range $10 \leq R_{\rm G} \leq 40$ kpc, searching in their surroundings for the stellar remnants of their accreted dwarf galaxy progenitors. We have detected a subjacent stellar populations beyond 1.5 times the $r_{\rm t}$ from the centre of 6 out the 23 GCs in our sample, and for three other clusters we found hints of possible

debris. These populations are in some cases consistent with known streams in the same line-of-sight of the GCs, while in other cases these over-densities might be associated with extended halos or tidal tails. Unfortunately our data do not cover a region wide enough to detect the full extension of the observed overdensities and their symmetry with respect to the cluster centre.

We identify the Sgr tidal stream in the direction of 6 GCs in our sample (4 "probable", 1 "possible" and 1 "uncertain" detection) and at distances compatible with the P10 orbital model. However, the heliocentric distances to the subjacent populations are consistent with those of the related GCs only for 2 of them (Whiting 1 and NGC 7492). Around NGC4147, NGC 5634 and Pal 5 (and with a smaller level of significance NGC 5053), previously suggested as members of the Sgr GC system, there are no significant detections corresponding to the same cluster distance, although the signature of the Sgr MS is visible as a background feature. These negative detections might be related with our ability of unveiling faint subjacent tidal streams (at $\mu_V > 32\,\mathrm{mag\,sec^{-2}}$). It is possible that these globulars were accreted from the Sgr dSph a long time ago and the surface-brightness of the tidal remnants lies beyond our detection threshold above the fore/background populations. On the contrary, Whiting 1 and NGC 7492 seem to be immersed in the most recently accreted fraction of the stream ($< 0.75\,\mathrm{Gyr}$). Follow-up spectroscopy is needed to confirm the nature of the stellar population revealed by our photometry, more importantly in the latter case, where the detection is more uncertain and there exists a significant deviation between the radial velocities of the cluster and the prediction of the model by P10.

A subjacent stellar population has been also unveiled in the surroundings of NGC 1851, NGC1261 and (possibly) NGC7006. These clusters lie far from the Sgr predicted orbit and could be therefore related to other streams like the Monoceros ring (NGC1851) the Hercules-Aquila cloud (NGC7006) or other unknown debris.

Acknowledgements

Based on observations made with the Isaac Newton Telescope operated on the island of La Palma by the Isaac Newton Group in the Spanish Observatorio del Roque de los Muchachos of the Instituto de Astrofísica de Canarias and with 2.2 m ESO telescope at the La Silla Observatory under programme IDs 072.A-9002(A), 082.B-0386, 084.B-0666 and 085.B-0765. JC-B received partial support from Centre of Excellence in Astrophysics and Associated Technologies (PFB 06). AS acknowledges the PRIN MIUR 2010-2011 "The Chemical and Dynamical Evolution of the Milky Way and Local Group Galaxies" (PI. Matteucci). RL acknowledges financial support to the DAGAL network from the People Programme (Marie Curie Actions) of the European Unions Seventh Framework Programme FP7/2007- 2013/ under REA grant agreement number PITN-GA-2011-289313. R. R. M. acknowledges partial support from CONICYT Anillo project ACT-1122 and project BASAL PFB-06 as well as FONDECYT project N°1120013. JMC-S acknowledges financial support to CONICYT through the FONDECYT Postdoc-

toral Fellowship N°3140310. We warmly thank the anonymous referee for his/her helpful comments and suggestions. We thank J. Peñarrubia for allowing us to use the model of the Sagittarius tidal stream for this work. Thanks to A. Robin for her useful comments about the Besançon model. Thanks to A. Aparicio, S. Hidalgo, R. Carrera and D. C. Bardalez-Gagliuffi for their participation in the observing runs.